

# Representation independent algorithms for molecular response calculations in time-dependent self-consistent field theories

Sergei Tretiak,<sup>1,2,a)</sup> Christine M. Isborn,<sup>3</sup> Anders M. N. Niklasson,<sup>1</sup> and Matt Challacombe<sup>1,b)</sup>

<sup>1</sup>Theoretical Division, Los Alamos National Laboratory, Los Alamos, New Mexico 87545, USA

<sup>2</sup>Center for Nonlinear Studies, and Center for Integrated Nanotechnologies, Los Alamos National Laboratory, Los Alamos, New Mexico 87545, USA

<sup>3</sup>Department of Chemistry, University of Washington, Box 351700, Seattle, Washington 98195-1700, USA

(Received 17 October 2008; accepted 28 November 2008; published online 4 February 2009)

Four different numerical algorithms suitable for a linear scaling implementation of time-dependent Hartree–Fock and Kohn–Sham self-consistent field theories are examined. We compare the performance of modified Lanczos, Arooldi, Davidson, and Rayleigh quotient iterative procedures to solve the random-phase approximation (RPA) (non-Hermitian) and Tamm–Dancoff approximation (TDA) (Hermitian) eigenvalue equations in the molecular orbital-free framework. Semiempirical Hamiltonian models are used to numerically benchmark algorithms for the computation of excited states of realistic molecular systems (conjugated polymers and carbon nanotubes). Convergence behavior and stability are tested with respect to a numerical noise imposed to simulate linear scaling conditions. The results single out the most suitable procedures for linear scaling large-scale time-dependent perturbation theory calculations of electronic excitations. © 2009 American Institute of Physics. [DOI: 10.1063/1.3068658]

## I. INTRODUCTION

Quantum mechanical treatment of molecular ground states involving numerical solution of the Schrödinger equation is a well-developed problem. Typical methods include Hartree–Fock (HF), density functional theory (DFT), and many sophisticated post-HF correlated wave function methods. Each method approaches the many-electron problem with a very specific technique.<sup>1–3</sup> These techniques provide important information about molecular geometry, chemical energy, distribution of the electronic density, etc. The bottleneck for quantum-mechanical methods in their application to large molecules is the scaling of the numerical cost with molecular size. Formally, HF and DFT Kohn–Sham self-consistent field (SCF) methods scale as  $\mathcal{O}(N^4)$ , where  $N$  is related to the number of basis functions, assumed to be proportional to molecular size. Substantial effort has been devoted toward the development of numerically efficient algorithms providing reduced computational cost. Linear  $\mathcal{O}(N)$  scaling has been achieved for ground state HF and DFT calculations.<sup>4–13</sup> Recently, a linear scaling solution of the coupled-perturbed SCF equations was formulated and was extended to the computation of higher-order static response properties<sup>14–18</sup> based on linear scaling density matrix perturbation theory.<sup>19</sup>

Another important area of molecular modeling is simulation of electronic excitations and the resonant frequency-dependent response. When a molecule is subjected to an external electromagnetic field, such as laser light, its electronic

density becomes time-dependent with dynamics involving excited electronic states. These excited state calculations are more involved compared to the ground state calculations due to many-body interactions (electronic correlations). A number of computational methodologies have been developed to deal with these issues, including the sophisticated multiple-determinant configuration interaction (CI) and coupled cluster schemes, equations of motion, and other many-body approaches such as Green's function approaches via the solution of the Bethe–Salpeter equation.<sup>1,3,20</sup> Among these approaches, simple and practical techniques such as the CI singles (CIS) and the time-dependent HF (TD-HF) theory, have been widely applied to molecular modeling. For example, coupled with simplified semiempirical Hamiltonian models (e.g., Pariser–Par–Pople or Zerner's intermediate neglect of differential overlap), these methods have been routinely used to calculate electronic excitations of large molecular systems for many years.<sup>21–23</sup> More than a decade ago, the TD-HF technique was extended to the more general hybrid HF/DFT models, and the time-dependent SCF (TD-SCF) method, which spans the range between adiabatic time-dependent DFT (TD-DFT) and TD-HF limits, has emerged.<sup>24–27</sup> This approach deals only with the one-electron density matrix, and has become a workhorse for the computation of excited state properties in nanosized materials.<sup>28–32</sup> Advances in the development of new density functionals has, so far, continuously improved accuracy in the computation of electronic excitations in molecular materials.

Solution of the TD-SCF equations in the frequency domain leads to the random-phase approximation (RPA) eigenvalue problem,<sup>33–36</sup> in this article, we focus on efficient numerical solution of this problem. Formally, the numerical cost of diagonalizing the TD-SCF equations scales as  $\mathcal{O}(N^6)$ ,

<sup>a)</sup>Electronic mail: serg@lanl.gov. URL: <http://www.t12.lanl.gov/home/serg>.

<sup>b)</sup>Electronic mail: mchalla@lanl.gov. URL: <http://www.t12.lanl.gov/home/mchalla>.

since the dimension of the RPA matrix is tetradic ( $N^2 \times N^2$ ) due to inclusion of Coulomb matrix elements necessary to account for electron–electron interactions. Over the years, a number of effective Krylov subspace algorithms and iterative techniques have been developed (e.g., Davidson algorithm).<sup>23,37–41</sup> Using direct methods for building the Fock (or Kohn–Sham) operator, these approaches are able to efficiently calculate the portion of the eigenspectrum of the RPA matrix necessary for modeling electronic excitations and optical response. Such diagonalizers became common in nearly all modern quantum-chemical codes, generally reaching  $\mathcal{O}(N^3)$ – $\mathcal{O}(N^4)$  complexity for excited state calculations. Utilizing sparse algebra techniques and modern direct Fock (or Kohn–Sham) operator builders,  $\mathcal{O}(N)$  scaling computational complexity for excited state calculations is feasible. However, for  $\mathcal{O}(N)$  scaling, all calculations should be done in the local atomic orbital (AO) representation, since the numerical expense for the molecular orbital (MO) representation, convenient for standard solution of the RPA problem, scales as  $\mathcal{O}(N^3)$ . Furthermore, the method should be applicable to the  $J$ -symmetric non-Hermitian structure of the RPA eigenproblem<sup>33,35,36</sup> and demonstrate convergence and stability with respect to the numerical noise resulting from the incomplete linear algebra employed to achieve  $\mathcal{O}(N)$  scaling.<sup>4–13</sup> A number of recent efforts have been devoted to the development of linear scaling orbital-free algorithms for calculation of excited states and dynamic (hyper) polarizabilities.<sup>42–48</sup> Even though there have been many recent developments of DFT-based approaches for solids utilizing plane wave (PW) basis,<sup>49–51</sup>  $\mathcal{O}(N)$  calculations remain challenging and require localized Wannier functions for ground state calculations. Moreover, computation of correlated excited states in PW framework remains problematic due to long-range exchange effects.<sup>20,52</sup>

In this article we test four different iterative algorithms for solution of the TD-SCF equations formulated in the orbital-free representation: modified Lanczos, Arnoldi, Davidson, and Rayleigh quotient iteration (RQI) procedures. Reference 53 represents the initial attempt by the present authors, where only the Rayleigh quotient method was attempted in the model system. The present work goes beyond the RQI method and compares its performance with three other Krylov subspace methods for several realistic molecules of different sizes. Semiempirical Hamiltonian models are chosen as a model chemistry. To simulate inexact algebra conditions inherent in the sparse matrix linear scaling approaches, we benchmark these algorithms under imposed numerical noise and analyze in detail their comparative performance. Section II introduces the underlying TD-SCF theoretical formalism, Sec. III presents the orbital-free algorithms considered, and Sec. IV analyzes the results of our numerical tests. Finally we discuss the trends that emerge and summarize our results in Sec. V.

## II. THEORETICAL METHODOLOGY

### A. TD-SCF framework

To introduce the time-dependent SCF theory spanning TD-HF (Refs. 33, 35, and 36) and adiabatic TD-DFT (Refs.

25 and 26) approaches, we start from a von-Neumann-type equation of motion of a single-electron density matrix  $\mathcal{P}(t) = \mathbf{P} + \delta\mathcal{P}(t)$ :<sup>54</sup>

$$i \frac{\partial \mathcal{P}}{\partial t} = [\mathbf{F}, \mathcal{P}] + [\mathbf{R}(t), \mathcal{P}], \quad (1)$$

where  $\mathbf{F}(\mathbf{P})$  is the effective single-particle Hamiltonian, i.e., the Fockian (or the Kohn–Sham Hamiltonian in DFT),  $\mathbf{P}$  is the ground state density matrix, and  $\mathbf{R}(t)$  is an external perturbation (e.g., induced by an external optical field). Square brackets denote the usual commutator,  $[\mathbf{F}, \mathcal{P}] = \mathbf{F}\mathcal{P} - \mathcal{P}\mathbf{F}$ . For brevity, here and everywhere, we assume an orthogonal representation, i.e., an orthogonal AO basis is defined, for instance, by Löwdin decomposition of the overlap matrix  $\mathbf{S}$ .<sup>1</sup>

Looking at the first-order response to perturbation  $\mathbf{R}(t)$  under variation of the density matrix  $\delta\mathcal{P}(t)$ , which contains the sought-out information about observables, such as frequency-dependent responses, we find that

$$i \frac{\partial \delta\mathcal{P}}{\partial t} = \mathbb{L}(\delta\mathcal{P}) + [\mathbf{R}(t), \mathcal{P}], \quad (2)$$

where

$$\mathbb{L}(\mathbf{x}) \equiv [\mathbf{F}, \mathbf{x}] + [\mathbf{G}(\mathbf{x}), \mathcal{P}] \quad (3)$$

is a tetradic Liouville superoperator,<sup>23,54</sup> and  $\mathbf{G}(\mathbf{x})$  is the Coulomb-exchange operator. Consequently, time-dependent evolution of  $\mathcal{P}(t)$  can be expanded via eigensolutions of  $\mathbb{L}$  in the limit of weak perturbations  $\mathbf{R}(t)$ . This is typical for quantum-chemical modeling dealing with finite molecular systems. Alternatively,  $\mathcal{P}(t)$  can be obtained by propagating Eq. (2) directly in real time,<sup>55–58</sup> which is a common approach in solid-state physics or in the limit of strong fields.<sup>28,31,59</sup>

In the general framework applicable to TD-HF, adiabatic TD-DFT techniques or their hybrid mixture,<sup>3,24</sup> the matrix elements of the Fock (or Kohn–Sham) operator  $\mathbf{F}(\mathbf{P})$  are given by

$$F_{ij\sigma}(\mathbf{P}) = t_{ij\sigma} + J_{ij\sigma}(\mathbf{P}) - K_{ij\sigma}(\mathbf{P}) + v_{ij\sigma}^{\text{xc}}(\mathbf{P}), \quad (4)$$

where the Coulomb and HF exchange terms are represented as

$$\begin{aligned} J_{ij\sigma}(\mathbf{P}) - K_{ij\sigma}(\mathbf{P}) &= \sum_{kl\sigma'} (ij\sigma|kl\sigma') P_{kl\sigma'} \\ &\quad - c_x (ik\sigma|jl\sigma') P_{kl\sigma} \delta_{\sigma\sigma'}. \end{aligned} \quad (5)$$

Here indices  $i, j, k, l$ , and  $\sigma$  refer to the spatial orbitals and the spin space, respectively.  $t_{ij\sigma}$  are one-electron integrals accounting for the kinetic energy and nuclear attraction of an electron, and  $(ij\sigma|kl\sigma')$  are conventional two-electron integrals representing Coulombic interactions. The exchange-correlation potential  $v^{\text{xc}}$ , given by a functional derivative of the exchange-correlation action  $A^{\text{xc}}$  in the DFT approach,<sup>25–27</sup> vanishes in HF theory. The hybrid mixing parameter  $c_x$  accounts for the amount of HF exchange in  $\mathbf{F}(\mathbf{P})$ . This parameter allows interpolation between pure DFT ( $c_x = 0$ ) and HF ( $c_x = 1$  and  $A^{\text{xc}} = 0$ ) theories. The total Coulomb-exchange term is defined as

$$G_{ij\sigma}(\mathbf{x}) = J_{ij\sigma}(\mathbf{x}) - K_{ij\sigma}(\mathbf{x}) + \sum_{kl\sigma'} f_{ij\sigma,kl\sigma'}^{\text{xc}} \mathbf{x}_{kl\sigma'}, \quad (6)$$

where the  $f^{\text{xc}}$  kernel is a functional derivative of the exchange-correlation potential  $v^{\text{xc}}$  in the DFT approach. Note that in Eqs. (4)–(6) the indices  $i, j, k, l, \sigma$  run over all basis functions  $\{\chi(\mathbf{r})\}$  irrespectively of representation. In a representation-free approach, the action of  $\mathbb{L}$  onto  $\mathbf{x}$  in Eq. (3) can be computed in the  $\mathcal{O}(N)$  regime using previously developed efficient Fock build procedures.<sup>4–9</sup>

## B. RPA eigenproblem

The eigenspectrum of the Liouville operator  $\mathbb{L}$  in Eq. (3) is given by the  $N^2 \times N^2$  eigenvalue problem

$$\mathbb{L}\vec{v} = \Omega\vec{v}, \quad (7)$$

where the vector  $\vec{v}$  is dyadic, corresponding to the unrolled  $N \times N$  matrix  $\mathbf{v}$ , i.e.,  $\mathbf{v}_{N \times N} \leftrightarrow \vec{v}_{N^2 \times 1}$ , where the double-headed arrow denotes both equivalence and a tensorial mapping.<sup>60</sup>

Traditionally, MOs provide a convenient representation allowing trivial decomposition of all possible transitions among occupied (hole, h) and virtual (particle, p) orbitals. A complete eigenspectrum of  $\mathbb{L}$  in Eq. (7) thus includes two distinct classes [i.e., interband (ph, hp) and intraband (pp, hh)] of transitions. Only “through-gap” electronic excitations related to the interband transitions are of interest for modeling spectroscopic observables.<sup>23</sup> Consequently, Eq. (7) is frequently recast in the MO representation as

$$\begin{pmatrix} \mathbf{A} & \mathbf{B} \\ -\mathbf{B} & -\mathbf{A} \end{pmatrix} \begin{pmatrix} \vec{X} \\ \vec{Y} \end{pmatrix} = \Omega \begin{pmatrix} \vec{X} \\ \vec{Y} \end{pmatrix}, \quad (8)$$

which is known as the RPA eigenvalue equation.<sup>61–64</sup> The eigenvalues of Eq. (8) represent vertical transition energies from the ground state to the excited states, entering as the poles of the linear response function of the system [see Eq. (2)]. The submatrices  $\mathbf{A}$  and  $\mathbf{B}$  are fourth-order tensors, i.e., they have a superoperator structure defined on the Liouville space  $(N_{\text{occ}}N_{\text{virt}}) \times (N_{\text{occ}}N_{\text{virt}})$ . Here  $N_{\text{occ}}$  and  $N_{\text{virt}}$  denote the Hilbert spaces of occupied and virtual molecular orbitals, respectively, with  $N = N_{\text{occ}} + N_{\text{virt}}$ . The tetradic elements of these matrices can always be chosen to be real and are given in the canonical MO basis as<sup>26,32,41</sup>

$$A_{ia\sigma, jb\sigma'} = (\varepsilon_{a\sigma} - \varepsilon_{i\sigma}) \delta_{ij} \delta_{ab} \delta_{\sigma\sigma'} + (ia\sigma|jb\sigma') + f_{ia\sigma, jb\sigma'} - c_x(ab\sigma|ij\sigma) \delta_{\sigma\sigma'}, \quad (9)$$

$$B_{ia\sigma, jb\sigma'} = (ia\sigma|jb\sigma') + f_{ia\sigma, jb\sigma'} - c_x(ja\sigma|ib\sigma) \delta_{\sigma\sigma'}, \quad (10)$$

where indices  $i, j$  ( $a, b$ ) run over occupied (virtual) molecular orbitals,  $\varepsilon_a$  and  $\varepsilon_i$  denote energies of molecular orbitals (Fockian eigenenergies), and the other quantities have been introduced in Eqs. (5) and (6).

In Eq. (8) the matrix  $\mathbf{A}$  is Hermitian and identical to the CISs matrix. Neglecting the Hermitian matrix  $\mathbf{B}$  results in the diagonalization of the  $\mathbf{A}$  operator, which gives the CIS excitation energies for a HF Hamiltonian, and is known as the Tamm-Dancoff (TDA)<sup>61,65,66</sup> when a DFT Hamiltonian is used. In this work, we examine algorithms for solving both

the RPA eigenproblem, and the corresponding  $\mathbf{B}=0$  problem, which we will denote as the TDA.  $\mathbf{A}$  is a diagonally dominant matrix for typical molecules. This provides efficient preconditioning schemes for various MO space algorithms. The first term of  $\mathbf{A}$  in Eq. (9), which is equivalent to the first term for the Liouville operator in Eq. (3), gives a “zero order” approximation to the excitation energies. If only this part is included in  $\mathbb{L}$ , the eigenvalues of Eq. (7) are simply the energy differences between the Fockian eigenvalues, i.e., the single-particle excitation energies corresponding to Koopmans theorem. The rest of the elements of  $\mathbf{A}$  and  $\mathbf{B}$  [i.e., the second term for the Liouville operator in Eq. (3)] include additional Coulomb and exchange-correlation screening of the excitation process.

Eigensolutions of Eq. (8) have a paired structure due to the  $J$ -symmetry of  $\mathbb{L}$  in the interband subspace:

$$\mathbb{L}\vec{v}_\alpha^+ = \Omega_\alpha \vec{v}_\alpha^+, \quad \mathbb{L}\vec{v}_\alpha^- = -\Omega_\alpha \vec{v}_\alpha^-, \quad (11)$$

where  $\alpha = 1, \dots, N_{\text{occ}} \times N_{\text{virt}}$  and the matrix transpose relates positive and negative transition density matrices (eigenvectors)  $\vec{v}_\alpha^- = (\vec{v}_\alpha^+)^T$ , which can always be chosen as real values. These paired eigensolutions of Eq. (8) [or Eq. (7) in the interband ph, hp subspace] correspond to excitation and de-excitation processes across the gap, which may be optically activated. The  $X$  and  $Y$  components of the eigenvector  $\vec{v}^+ = \begin{pmatrix} \vec{X} \\ \vec{Y} \end{pmatrix}$  ( $\vec{v}^- = \begin{pmatrix} \vec{Y} \\ \vec{X} \end{pmatrix}$ ) in the MO representation are, respectively, the particle-hole (ph) and hole-particle (hp) components. For a majority of molecules, the  $\vec{X}$  component dominates (i.e.,  $\|\vec{X}\| \gg \|\vec{Y}\|$ ), because elements of supermatrix  $\mathbf{B}$  represent higher-order electronic correlations and their magnitudes are small compared to those of matrix  $\mathbf{A}$ . Consequently, the TDA ( $\mathbf{B}=0$ ,  $\vec{Y}=0$ ) is considered as a good approximation and is widely used for the original RPA problem.

## C. Representation independent formalism

Conventional orbital based algorithms for solving the TD-SCF equations restrict the solution subspace to ph-hp symmetry by construction. In an orbital independent formulation, this ph-hp symmetry can be imposed using the occupied subspace projector  $\mathbf{P}$  (the idempotent ground state density matrix) and its complement,  $\mathbf{Q} = \mathbf{I} - \mathbf{P}$ , with the projection scheme<sup>1,67–71</sup>

$$\mathbf{x}_P = \mathbf{P}\mathbf{x}\mathbf{Q} + \mathbf{Q}\mathbf{x}\mathbf{P}. \quad (12)$$

or equivalently

$$\mathbf{x}_P = [[\mathbf{x}, \mathbf{P}], \mathbf{P}]. \quad (13)$$

The first and the second terms in Eq. (12) provide projection into ph and hp subspaces, respectively. For large and sparse problems, it is possible to construct these projectors in  $\mathcal{O}(N)$  using recursive purification methods.<sup>67,72,73</sup>

The unitary matrix  $\mathbb{N} = \begin{pmatrix} \mathbf{I} & 0 \\ 0 & -\mathbf{I} \end{pmatrix}$ , implicitly present in Eq. (8), is a metric tensor defining the indefinite inner product associated with the Liouville space.<sup>74</sup> In a general representation this metric can be applied implicitly through the projection

$$\vec{x}_N = \mathbb{N}\vec{x} \Leftrightarrow (\mathbf{P} - \mathbf{Q})\mathbf{x}_p, \quad (14)$$

which is valid only in the ph-hp subspace. We note that for the real matrices encountered in quantum chemistry  $\mathbf{x}^\dagger = \mathbf{x}^T$ , which in an orbital representation is equivalent to the transfer operation  $\begin{pmatrix} \vec{x} \\ \vec{y} \end{pmatrix} \rightarrow \begin{pmatrix} \vec{y} \\ \vec{x} \end{pmatrix}$ . The corresponding indefinite inner product between arbitrary vectors  $\vec{x}$  and  $\vec{y}$  in the Liouville space is then given as<sup>23,36,74</sup>

$$\langle \vec{x}, \vec{y} \rangle = \text{Tr}\{\mathbf{x}^T(\mathbf{P} - \mathbf{Q})\mathbf{y}\} \quad (15a)$$

$$= \text{Tr}\{\mathbf{x}^T[\mathbf{y}, \mathbf{P}]\}, \quad (15b)$$

an equivalence that holds only within the ph-hp subspace. To avoid confusion, hereafter we will only consider vectors and matrices belonging to the ph-hp space, assuming that they result from the projection given by Eq. (12), and the subscript  $P$  is dropped henceforth.

The scalar product (15) can be used to introduce the orthogonality relation between eigenvectors  $\vec{v}_\alpha$  and  $\vec{v}_\beta$  as

$$\langle \vec{v}_\alpha, \vec{v}_\beta \rangle = \text{Tr}\{\mathbf{v}_\alpha^T(\mathbf{P} - \mathbf{Q})\mathbf{v}_\beta\} = \delta_{\alpha\beta}. \quad (16)$$

This scalar product is *antisymmetric* with respect to exchange of  $\vec{v}_\alpha^+$  for  $\vec{v}_\alpha^-$ :  $\langle \vec{v}_\alpha^+ | \vec{v}_\alpha^+ \rangle = -\langle \vec{v}_\alpha^- | \vec{v}_\alpha^- \rangle$ . In an orbital representation, Eq. (16) is equivalent to the familiar expression  $\vec{X}_\alpha \cdot \vec{X}_\beta - \vec{Y}_\alpha \cdot \vec{Y}_\beta = \delta_{\alpha\beta}$ . It reduces to the usual dot product between vectors  $\vec{X}_\alpha$  and  $\vec{X}_\beta$  in the TDA approximation ( $\vec{v} = \begin{pmatrix} \vec{x} \\ 0 \end{pmatrix}$ ).

As shown by Thouless<sup>74</sup> in 1961, eigensolutions of the RPA Eq. (8) can be found variationally. Given the above definitions, the Thouless functional can be written as

$$\Omega[\vec{x}] = \frac{\langle \vec{x}, \mathbb{L}\vec{x} \rangle}{|\langle \vec{x}, \vec{x} \rangle|}. \quad (17)$$

In the TDA, this functional reduces to the usual Ritz functional for Hermitian operators  $\Omega[\vec{x}] = \vec{x} \cdot \mathbf{A}\vec{x} / \vec{x} \cdot \vec{x}$ . Both Thouless and Ritz functionals can be optimized in variational algorithms to find eigensolutions.

### D. Coordinate-momentum representation

We note that Eq. (2) can be envisioned as an equation of motion for coupled harmonic oscillators. In particular, the TD-SCF approximation is usually considered as a classical limit of the original many-electron system.<sup>23,75</sup> Each oscillator  $\alpha$  ( $\alpha = 1, \dots, N_{\text{occ}} \times N_{\text{virt}}$ ) is described by two conjugate modes  $\vec{v}_\alpha^+ = \begin{pmatrix} \vec{X}_\alpha \\ \vec{Y}_\alpha \end{pmatrix}$  and  $\vec{v}_\alpha^- = \begin{pmatrix} \vec{Y}_\alpha \\ \vec{X}_\alpha \end{pmatrix}$ . It is frequently advantageous to consider transformation to the coordinate-momentum variables  $\{\mathbf{q}, \mathbf{p}\}$  as

$$\vec{q}_\alpha = \vec{X}_\alpha + \vec{Y}_\alpha \quad \text{and} \quad \vec{p}_\alpha = \vec{X}_\alpha - \vec{Y}_\alpha. \quad (18)$$

The orthonormalization relation (16) then reduces to the usual dot product between eigenvectors  $\vec{p}_\alpha$  and  $\vec{q}_\beta$

$$\vec{p}_\alpha \cdot \vec{q}_\beta = \delta_{\alpha\beta}. \quad (19)$$

The RPA eigenvalue problem [Eq. (11)] in these variables is given as

$$(\mathbf{A} - \mathbf{B})\vec{p}_\alpha = \Omega_\alpha \vec{q}_\alpha, \quad (\mathbf{A} + \mathbf{B})\vec{q}_\alpha = \Omega_\alpha \vec{p}_\alpha. \quad (20)$$

That is,

$$\begin{pmatrix} 0 & \mathbf{K} \\ \mathbf{T} & 0 \end{pmatrix} \begin{pmatrix} \vec{p} \\ \vec{q} \end{pmatrix} = \Omega \begin{pmatrix} \vec{p} \\ \vec{q} \end{pmatrix}. \quad (21)$$

Here the Hermitian superoperators  $\mathbf{K} = \mathbf{A} + \mathbf{B}$  and  $\mathbf{T} = \mathbf{A} - \mathbf{B}$  are the stiffness and kinetic energy matrices, respectively. Notably, both matrices  $\mathbf{K}$  and  $\mathbf{T}$  are diagonally dominant. Furthermore, Eq. (20) can be rewritten in two forms:

$$\mathbf{T}\mathbf{K}\vec{q}_\alpha = \Omega_\alpha^2 \vec{q}_\alpha \quad \text{or} \quad \mathbf{K}\mathbf{T}\vec{p}_\alpha = \Omega_\alpha^2 \vec{p}_\alpha, \quad (22)$$

and

$$\mathbf{T}^{1/2}\mathbf{K}\mathbf{T}^{1/2}\vec{q}'_\alpha = \Omega_\alpha^2 \vec{q}'_\alpha \quad \text{or} \quad \mathbf{K}^{1/2}\mathbf{T}\mathbf{K}^{1/2}\vec{p}'_\alpha = \Omega_\alpha^2 \vec{p}'_\alpha \quad (23)$$

where  $\vec{q}'_\alpha = \mathbf{T}^{-1/2}\vec{q}_\alpha$  and  $\vec{p}'_\alpha = \mathbf{K}^{-1/2}\vec{p}_\alpha$ . Both Eqs. (22) and (23) are  $N_{\text{occ}} \times N_{\text{virt}}$  Hermitian problems, which have been utilized in the Davidson solver for RPA problem.

The action of operators  $\mathbf{K}$  and  $\mathbf{T}$  on an arbitrary ph vector  $\vec{x} = \begin{pmatrix} \vec{x} \\ 0 \end{pmatrix}$  can be computed directly using Eqs. (3) and (12) as

$$(\mathbf{A} + \mathbf{B})\mathbf{x} = \mathbf{K}\mathbf{x} = \mathbf{P}\mathbb{L}\mathbf{x}\mathbf{Q} - (\mathbf{Q}\mathbb{L}\mathbf{x}\mathbf{P})^T, \quad (24)$$

$$(\mathbf{A} - \mathbf{B})\mathbf{x} = \mathbf{T}\mathbf{x} = \mathbf{P}\mathbb{L}\mathbf{x}\mathbf{Q} + (\mathbf{Q}\mathbb{L}\mathbf{x}\mathbf{P})^T, \quad (25)$$

where the resulting vectors belong to the ph subspace as well. These relations can be easily rationalized from  $\mathbb{L}\vec{x} = \mathbb{L}\begin{pmatrix} \vec{x} \\ 0 \end{pmatrix} = \begin{pmatrix} \mathbf{A}\vec{x} \\ -\mathbf{B}\vec{x} \end{pmatrix}$ .

Optimization of the Thouless functional Eq. (17) in  $\mathbf{q} - \mathbf{p}$  variables corresponds to finding the lowest frequency of a harmonic Hamiltonian system over all phase-space configurations  $\{\mathbf{q}, \mathbf{p}\}$ , normalized by  $\vec{p} \cdot \vec{q} = 1$ .<sup>76,77</sup>

$$\Omega[\vec{p}, \vec{q}] = \min_{\vec{p} \cdot \vec{q} = 1} \left\{ \frac{\vec{p} \cdot \mathbf{T}\vec{p}}{2} + \frac{\vec{q} \cdot \mathbf{K}\vec{q}}{2} \right\}. \quad (26)$$

### III. ORBITAL-FREE ALGORITHMS

With the above developments, we now formulate several representation-independent algorithms. The first three algorithms outlined here—Lanczos, Arnoldi, and Davidson—belong to a family of so-called Krylov subspace iterative methods. A Krylov subspace is spanned by the iterates of simple power methods.<sup>78–80</sup> These three algorithms are among the most successful methods for extracting a partial eigenspectrum of large (frequently sparse) matrices. The RQI technique involves unconstrained nonlinear optimization following the gradient of the excitation energy. All four algorithms differ from the original parent procedures<sup>78–80</sup> because of the requirements of the  $J$ -symmetry of  $\mathbb{L}$  [Eq. (8)] and the Thouless variational principle [Eq. (17)].<sup>74</sup> Reduction in the RPA problem into a simpler Hermitian TDA approximation, subject to the Ritz variational principle, is achieved by constraining all calculations to the ph subspace only [i.e., to the first term in Eq. (12)].

For simplicity, all algorithms target the first positive eigenvalue and corresponding eigenvector in Eq. (7). Generally, it is numerically advantageous to iterate several eigen-

states at once (block iterations). We illustrate this approach in an example of the Davidson algorithm in Sec. IV. Such extensions are possible for other procedures as well.<sup>78</sup> Notably, if too many states are obtained simultaneously, efficiency degrades due to enhanced memory and I/O requirements. Consequently, eigenstates may be found one by one or in small batches of optimal size. Finding subsequent eigenstates requires that lower lying eigenvectors are either projected out or shifted away, so that they are not rediscovered by minimization. Here, we consider the symmetric Wilkinson shift<sup>81</sup> of the calculated interior eigenvalues to the new values  $\Omega_j + \sigma_j$ , which are outside the region of interest, written as the shifted  $\mathbb{L}\vec{x}$ :

$$\mathbb{L}^{\text{sh}}\vec{x} = \mathbb{L}\vec{x} + \sum_j^k \varsigma_j \{v_j \langle \vec{v}_j, \vec{x} \rangle + \vec{v}_j^T \langle \vec{v}_j^T, \vec{x} \rangle\}, \quad (27)$$

where  $\{\vec{v}_j\}$  ( $j=1, \dots, k$ ) are previously determined eigenstate transition densities. In Eq. (27), the first and second terms in the square parentheses symmetrically shift up and down the positive and negative eigenvalues  $\Omega_j$  in the spectrum of the Liouville operator  $\mathbb{L}$  by an amount of  $\varsigma_j$ . For practical purposes, the latter values are chosen to be  $\varsigma_j = \Omega_k - \Omega_1 + \varsigma$ , where empirical parameter  $\varsigma$  should exceed the density of electronic states in the spectrum of a given molecule.

Finally, we note that the initial guesses for the eigenvectors are very important in every algorithm considered. One of the benefits of MO space is that it provides convenient and relatively accurate initial trial vectors for the transition density matrices as transitions between molecular orbitals, a so-called Koopmans's guess (for instance, the highest occupied molecular orbital (HOMO)-lowest unoccupied molecular orbital (LUMO) transition for the lowest excitation eigenvector). These guesses, however, are not readily available in an orbital-free algorithm. A simple random guess projected onto the total interband ph+hp subspace ( $\vec{x}_0 = \mathbf{P}\mathbf{x}\mathbf{Q} + \mathbf{Q}\mathbf{x}\mathbf{P}$ ) is vastly inefficient. Since the  $\vec{X}$  component dominates the  $\vec{Y}$  part of the eigenvector  $\vec{v} = \begin{pmatrix} \vec{X} \\ \vec{Y} \end{pmatrix}$ , a random guess projected onto only the ph subspace ( $\vec{x} = \mathbf{P}\mathbf{x}\mathbf{Q}$ ) is substantially advantageous in terms of both stability and convergence. This can be further improved by accounting for spatial (diagonal) locality of the matrices  $\mathbf{v}$ , i.e., by considering only diagonally dominant random guesses  $\vec{x}$  with subsequent projection onto the ph subspace. Finally, induced density matrices for higher-order static responses may provide more accurate initial guesses. These higher-order response terms  $\mathbf{P}^{(i)}$  in the expansion  $\mathcal{P} = \mathbf{P} + \mathbf{P}^{(1)} + \mathbf{P}^{(2)} + \dots$ , can be calculated efficiently,<sup>14–16,82</sup> using linear scaling density matrix perturbation theory.<sup>19,83</sup> It was shown how the density matrix response can be calculated to any order (to 10th order in an example in Ref. 19). Again, these quantities need to be projected onto the ph subspace to obtain the initial guesses. The effect of these initial guesses on the algorithm convergence and stability is tested in Sec. IV.

## A. Lanczos and Arnoldi algorithms

The Lanczos algorithm for a Hermitian eigenvalue problem is among the most common approaches for sparse

```

(1) for  $k = 1$  to  $K$  do
(2)   Generate trial vector,  $\vec{x}$ ,
(3)    $\mathbf{p}_0 = \mathbf{q}_0 = \mathbf{P}\mathbf{x}\mathbf{Q}$ 
(4)   if restart  $\mathbf{p}_0 = \mathbf{p}_i$ ,  $\mathbf{q}_0 = \mathbf{q}_i$  fi
(5)   for  $i = 0$ , until convergence or restart do
(6)      $\vec{s} = \mathbb{L}^{\text{sh}}\vec{p}_i$ ,  $\vec{t} = \mathbb{L}^{\text{sh}}\vec{q}_i$ 
(7)      $\mathbf{q}_{i+1} = \mathbf{P}\mathbf{s}\mathbf{Q} - (\mathbf{Q}\mathbf{s}\mathbf{P})^T$ ,  $\mathbf{p}_{i+1} = \mathbf{P}\mathbf{t}\mathbf{Q} + (\mathbf{Q}\mathbf{t}\mathbf{P})^T$ 
(8)      $\vec{q}_{i+1} = \vec{q}_{i+1} - \beta_i\vec{q}_{i-1}$ ,  $\vec{p}_{i+1} = \vec{p}_{i+1} - \delta_i\vec{p}_{i-1}$ 
(9)      $\tilde{K}_{i,i} = \alpha_i = \vec{p}_{i+1} \cdot \vec{q}_i$ ,  $\tilde{T}_{i,i} = \gamma_i = \vec{q}_{i+1} \cdot \vec{p}_i$ 
(10)     $\vec{q}_{i+1} = \vec{q}_{i+1} - \alpha_i\vec{q}_i$ ,  $\vec{p}_{i+1} = \vec{p}_{i+1} - \gamma_i\vec{p}_i$ 
(11)     $f = \vec{p}_{i+1} \cdot \vec{q}_{i+1}$ 
(12)     $\tilde{K}_{i,i+1} = \tilde{K}_{i+1,i} = \beta_{i+1} = \sqrt{|f|}$ 
(13)     $\tilde{T}_{i,i+1} = \tilde{T}_{i+1,i} = \delta_{i+1} = \text{sgn}\{f\}\beta_i$ 
(14)     $\vec{q}_{i+1} = \frac{\vec{q}_{i+1}}{\beta_{i+1}}$ ,  $\vec{p}_{i+1} = \frac{\vec{p}_{i+1}}{\delta_{i+1}}$ 
(15)    solve  $\tilde{\mathbf{T}}\vec{d} = \omega\vec{c}$ ,  $\tilde{\mathbf{K}}\vec{c} = \omega\vec{d}$ 
(16)     $\Omega = \min_{\omega_i > 0} \{\omega_i\}$ 
(17)     $\vec{p} = \sum_0^i d_i\vec{p}_i$ ,  $\vec{q} = \sum_0^i c_i\vec{q}_i$ 
(18)     $\mathbf{p} = \mathbf{P}\mathbf{p}\mathbf{Q}$ ,  $\mathbf{q} = \mathbf{P}\mathbf{q}\mathbf{Q}$ 
(19)     $\mathbf{v} = 0.5(\mathbf{q} + \mathbf{p} + (\mathbf{q} - \mathbf{p})^T)$ 
(20)     $\vec{v} = \frac{\vec{v}}{\sqrt{|\langle \vec{v}, \vec{v} \rangle|}}$ 
(21)     $\vec{w} = \mathbb{L}^{\text{sh}}\vec{v}$ 
(22)     $\mathbf{w} = \mathbf{P}\mathbf{w}\mathbf{Q} + \mathbf{Q}\mathbf{w}\mathbf{P}$ 
(23)     $\epsilon = \sum_{n=1}^{N^2} (\Omega\vec{v}_n - \vec{w}_n)^2$ 
(24)    if  $\epsilon < \eta$ ,  $\Omega_k = \Omega$ ,  $\vec{v}_k = \vec{v}$ , exit, fi
(25)  end
(26) end

```

SCHEME 1. Modified Lanczos algorithm.

eigenproblems.<sup>78</sup> A simple recursive procedure builds a set of orthogonal vectors spanning the Krylov subspace. Finding each new vector only requires the two previous vectors.<sup>80,84</sup> In search of efficient algorithms for the  $J$ -symmetric RPA problem, the symplectic Lanczos algorithm was suggested by Mei<sup>85</sup> and improved by Benner and Fassbender.<sup>86</sup> The oblique Lanczos algorithm for general non-Hermitian matrices<sup>78</sup> was applied to the TDHF problem in Ref. 87 and further improved in Refs. 76 and 77. The latter algorithm, which utilizes the Thouless variational principle [Eq. (26)] is described below.

Scheme 1 summarizes the Lanczos algorithm for the RPA problem [Eq. (8)],<sup>76,77</sup> which finds a few lowest eigenvalues of the Liouville matrix  $\mathbb{L}$ . The numerical procedure starts with two arbitrary vectors  $\vec{p}_0$  and  $\vec{q}_0$  [lines (2)–(4)] and constructs linear combinations of vectors  $(\mathbf{A} + \mathbf{B})^m(\mathbf{A} - \mathbf{B})^m\vec{p}_0$ , and  $(\mathbf{A} - \mathbf{B})^m(\mathbf{A} + \mathbf{B})^m\vec{q}_0$ ,  $m=0, 1, \dots, M$  forming the Krylov subspace [lines (5)–(25)]. The coefficients in this linear combination are found using the Thouless variational procedure which guarantees the best approximation to the

lowest eigenvalue of  $\mathbb{L}$  that belongs to a Krylov subspace. Specifically, the minimum of Eq. (26) can be found using the generalized Lanczos recursion<sup>76,77</sup>

$$\vec{q}_{m+1} = \beta_{m+1}^{-1}(\mathbf{T}^{sh}\vec{p}_m - \alpha_m\vec{q}_m - \beta_m\vec{q}_{m-1}), \quad (28)$$

$$\vec{p}_{m+1} = \delta_{m+1}^{-1}(\mathbf{K}^{sh}\vec{q}_m - \gamma_m\vec{p}_m - \delta_m\vec{p}_{m-1}), \quad m = 1, \dots, M, \quad (29)$$

which generates configuration space vectors  $\{\vec{q}_m, \vec{p}_m\}$  that span the Krylov subspace of Eq. (26). This subspace ( $\mathcal{K}_M$ ) approximates an invariant subspace of  $\mathbb{L}$  with increasing accuracy as the number of vectors is increased. The action of operators  $\mathbf{T}^{sh}$  and  $\mathbf{K}^{sh}$  on vectors  $p_m$  and  $q_m$  can be computed directly using Eqs. (24), (25), and (27), see lines (6) and (7) in Scheme 1. Coefficients  $\alpha_m$ ,  $\beta_m$ ,  $\gamma_m$ , and  $\eta_m$  are chosen at each step  $m$  to ensure orthogonality  $\vec{q}_{m+1} \cdot \vec{p}_m = \vec{q}_{m+1} \cdot \vec{p}_{m-1} = \vec{q}_{m-1} \cdot p_m = \vec{q}_{m-1} \cdot \vec{p}_{m+1} = 0$  according to the recursive relations (28) and (29) [lines (8), (10), (11), and (14)]. The vectors  $\vec{p}_m$  and  $\vec{q}_m$  thus form a biorthogonal basis,  $\vec{q}_n \cdot \vec{p}_m = \delta_{nm}$ , and the matrices  $\tilde{K}_{ij} = \vec{q}_i \cdot \mathbf{K} \vec{q}_j$  and  $\tilde{T}_{ij} = \vec{p}_i \cdot \mathbf{T} \vec{p}_j$  are symmetric tridiagonal, with the only nonzero matrix elements  $\tilde{K}_{ii} = \alpha_i$ ,  $\tilde{K}_{i,i-1} = \tilde{K}_{i-1,i} = \beta_i$ ,  $\tilde{T}_{ii} = \eta_i$ , and  $\tilde{T}_{i,i-1} = \tilde{T}_{i-1,i} = \gamma_i$  [lines (9), (12), and (13)]. Expanding  $\vec{q} = \sum_{m=1}^M c_m \vec{q}_m$  and  $\vec{p} = \sum_{m=1}^M d_m \vec{p}_m$  [line (17)], we obtain a  $2M \times 2M$  eigenvalue equation in the  $\mathcal{K}_M$  subspace [line (15)] which has the same structure as the original eigenproblem Eq. (20) but in a space of much lower dimensionality  $M$ . The lowest positive eigenvalue  $\Omega_{\min}$  of the reduced eigenproblem gives an approximation to the true RPA eigenfrequency [line (16)]. The respective approximate RPA eigenvector is formed using eigenvectors of the reduced problem [lines (17)–(20)]. Ideally, the accuracy increases exponentially with expanding Krylov space dimensionality and the iteration stops when the desired accuracy threshold is achieved [lines (21)–(24)]. The projection to the interband subspace needs to be adhered to throughout the entire procedure [lines (3), (7), (18), and (22)]. Finally we note that in the TDA framework, Eqs. (28) and (29) become identical (i.e.,  $\mathbf{T}^{sh} = \mathbf{K}^{sh} = \mathbf{A}^{sh}$ ) and the described generalized iterations reduce to the usual Lanczos algorithm.<sup>80,84</sup>

Similar to the Hermitian Lanczos method, the generalized Lanczos recursive iterations described above need to retain only the three latest pairs  $\{p_m, q_m\}$  of expansion vectors, which ensures minimal memory requirements for this procedure. However, for practical quantum-chemical applications, it is necessary to compute the RPA eigenvectors [line (17) in Scheme 1]. Consequently, all expansion vectors  $\{p_m, q_m\}$  need to be stored. Moreover, a significant drawback of Lanczos recursion is loss of orthogonality among the expansion vectors, which is a well-studied problem.<sup>79,88</sup> This issue becomes particularly severe in inexact algebra conditions due to propagation of numerical errors, as explored in Sec. IV. A simple solution is imposing an explicit orthogonalization of the expansion vectors, leading to the Arnoldi iterations. In the case of exact arithmetic, commonly used Hermitian Lanczos and Arnoldi procedures are identical.<sup>78,79</sup>

Scheme 2 summarizes the generalized Arnoldi algorithm for the RPA problem corresponding to the generalized Lanczos recursion described in Sec. II. Compared to Scheme 1,

```
(1) for  $k = 1$  to  $K$  do
(2)   Generate trial vector,  $\vec{x}$ ,
(3)    $\mathbf{p}_0 = \mathbf{q}_0 = \mathbf{P} \mathbf{x} \mathbf{Q}$ 
(4)   if restart  $\mathbf{p}_0 = \mathbf{p}_i$ ,  $\mathbf{q}_0 = \mathbf{q}_i$  fi
(5)   for  $i = 0$ , until convergence or restart do
(6)      $\vec{s} = \mathbb{L}^{sh} \vec{p}_i$ ,  $\vec{t} = \mathbb{L}^{sh} \vec{q}_i$ 
(7)      $\mathbf{q}_{i+1} = \mathbf{P} \mathbf{s} \mathbf{Q} - (\mathbf{Q} \mathbf{s} \mathbf{P})^T$ ,  $\mathbf{p}_{i+1} = \mathbf{P} \mathbf{t} \mathbf{Q} + (\mathbf{Q} \mathbf{t} \mathbf{P})^T$ 
(8)     for  $j = 0$  to  $i$  do
(9)        $\tilde{T}_{i,j} = \vec{q}_{i+1} \cdot \vec{p}_j$ ,  $\tilde{K}_{i,j} = \vec{p}_{i+1} \cdot \vec{q}_j$ 
(10)       $\vec{q}_{i+1} = \vec{q}_{i+1} - \sum_{j=0}^i \tilde{T}_{i,j} \vec{q}_j$ ,  $\vec{p}_{i+1} = \vec{p}_{i+1} - \sum_{j=0}^i \tilde{K}_{i,j} \vec{p}_j$ 
(11)     end
(12)      $f = \vec{p}_{i+1} \cdot \vec{q}_{i+1}$ 
(13)      $\vec{q}_{i+1} = \frac{\vec{q}_{i+1}}{\sqrt{|f|}}$ ,  $\vec{p}_{i+1} = \frac{\vec{p}_{i+1} \text{sgn}\{f\}}{\sqrt{|f|}}$ 
(14)     solve  $\tilde{\mathbf{T}} \vec{d} = \omega \vec{c}$ ,  $\tilde{\mathbf{K}} \vec{c} = \omega \vec{d}$ 
(15)      $\Omega = \min_{\omega_i > 0} \{\omega_i\}$ 
(16)      $\vec{p} = \sum_0^i d_i \vec{p}_i$ ,  $\vec{q} = \sum_0^i c_i \vec{q}_i$ 
(17)      $\mathbf{p} = \mathbf{P} \mathbf{p} \mathbf{Q}$ ,  $\mathbf{q} = \mathbf{P} \mathbf{q} \mathbf{Q}$ 
(18)      $\mathbf{v} = 0.5(\mathbf{q} + \mathbf{p} + (\mathbf{q} - \mathbf{p})^T)$ 
(19)      $\vec{v} = \frac{\vec{v}}{\sqrt{|\langle \vec{v}, \vec{v} \rangle|}}$ 
(20)      $\vec{w} = \mathbb{L}^{sh} \vec{v}$ 
(21)      $\mathbf{w} = \mathbf{P} \mathbf{w} \mathbf{Q} + \mathbf{Q} \mathbf{w} \mathbf{P}$ 
(22)      $\epsilon = \sum_{n=1}^{N^2} (\Omega \vec{v}_n - \vec{w}_n)^2$ 
(23)     if  $\epsilon < \eta$ ,  $\Omega_k = \Omega$ ,  $\vec{v}_k = \vec{v}$ , exit, fi
(24)   end
(25) end
```

SCHEME 2. Modified Arnoldi algorithm.

instead of recursions (28) and (29), the expansion vectors are explicitly orthogonalized utilizing a Gram–Schmidt algorithm [line (10)]. Moreover, reduced matrices  $\tilde{K}_{ij}$  and  $\tilde{T}_{ij}$  are no longer symmetric tridiagonal in inexact arithmetic conditions [line (9)]. This, of course, slightly increases numerical expense but avoids the severe loss of orthogonality that takes place in the Lanczos algorithm for inexact algebra.

## B. Davidson algorithm

Davidson’s algorithm, originally formulated for the Hermitian TDA problem, extensively utilizes the fact that the TDA supermatrix  $\mathbf{A}$  is diagonally dominant.<sup>37</sup> The resulting Davidson’s preconditioning is particularly simple in the MO representation. With such preconditioning the algorithm requires fewer iterations compared to similar methods. Similar to Lanczos and Arnoldi’s methods for solving the RPA problem, Davidson’s algorithm needs to be modified to take into account the block paired structure of Eq. (8) and the scalar product of Eq. (16). The first RPA algorithm was developed by Rettrup<sup>38</sup> and later improved by Olsen *et al.*<sup>39</sup> The method has been further refined and combined with the TDDFT tech-

nique in Ref. 41. Here we describe a variation of the Davidson method working with a block of vectors following Ref. 41.

Scheme 3 summarizes the Davidson algorithm for the RPA problem. To find  $K$  excited states simultaneously, the algorithm first generates  $2K$  trial vectors [line (1)] or utilizes guesses from the previous iterations as trial vectors [line (2)]. These trial vectors are further projected onto the ph subspace [line (3)] and orthonormalized using a standard dot product [line (6)]. For the ph subspace, the dot product coincides with the RPA scalar product Eq. (16). The Krylov configuration space  $(\mathbf{A} \pm \mathbf{B})\vec{x}_k$  is generated next [lines (8) and (9)] using Eqs. (24), (25), and (27), which is the most CPU intensive step. Consequently, line 12 computes the reduced analogs ( $\tilde{\mathbf{K}}$  and  $\tilde{\mathbf{T}}$ ) of stiffness  $\mathbf{K}=\mathbf{A}+\mathbf{B}$  and kinetic energy  $\mathbf{T}=\mathbf{A}-\mathbf{B}$  matrices for a given Krylov subspace dimension. These quantities, in turn, lead to the reduced RPA eigenproblem analogous to Eq. (23) [lines (14) and (15)]. Its eigenvalues provide approximations to the true RPA eigenfrequencies [line (18)], and the respective eigenvectors allow calculation of  $\tilde{\mathbf{L}}$  and  $\tilde{\mathbf{R}}$  [line (16)], which are reduced analogs of the RPA eigenvectors  $\mathbf{q}$  and  $\mathbf{p}$  in Eq. (20).  $\tilde{\mathbf{L}}$  and  $\tilde{\mathbf{R}}$  are thus expansion coefficients for the approximate  $\mathbf{q}$  and  $\mathbf{p}$  through the trial vectors [line (19)]. Approximate  $\mathbf{q}$  and  $\mathbf{p}$  eigenvectors obtained after projection [line (20)] and normalization [line (21)] to satisfy Eq. (19), are then used to calculate the approximation to the transition density [line (26)], residual vectors [lines (22)–(24)] and respective residual norms [line (25)]. These residual vectors are further used to augment the trial vector subspace [line (28)]. Similar to previously described algorithms, the accuracy increases exponentially with expanding Krylov space dimensionality and the iteration stops when the desired accuracy threshold is achieved [line (27)].

Note that, unlike in the original algorithm, we are not using preconditioning for the residual vectors ( $\Omega_k - \mathbb{L}^{(1)-1}(\vec{r}_k)$ ) to expand the trial vector subspace, where  $\mathbb{L}^{(1)}$  is a diagonal superoperator corresponding to the leading part of  $\mathbf{A}$  [first term in Eq. (9)]. The explicit form of the preconditioner is simply expressed through the energies of occupied  $\varepsilon_i$  and valence  $\varepsilon_a$  molecular orbitals [i.e.,  $((\Omega_k - \mathbb{L}^{(1)-1})_{aa'ii'})^{-1} = 1/(\Omega_k - \varepsilon_a + \varepsilon_i)\delta_{aa'}\delta_{ii'}$ ]. However, the inversion of the superoperator  $\mathbb{L}^{(1)}$  is no longer a simple task in an arbitrary representation. An alternative preconditioner form has been explored in Ref. 46. Designing an optimal preconditioning approach in MO-free representation is a subject for future studies. Our numerical tests in Sec. IV show that, even without preconditioning, the Davidson algorithm shows superior convergence and stability properties in inexact algebra compared to the other methodologies considered here.

### C. Rayleigh quotient optimization

We lastly outline the RQI algorithm following Ref. 53 which directly minimizes the Thouless functional [Eq. (17)] and involves unconstrained nonlinear optimization.<sup>89</sup> This approach belongs to a family of nonlinear conjugate gradient algorithms, which have the ability to reset and to proceed downhill in response to functional nonlinearities, and also

```

(1) Generate  $2K$  trial vectors,  $\vec{x}_1, \dots, \vec{x}_{2K}$ 
(2) if restart  $\mathbf{x}_{2k-1} = \mathbf{v}_k + \mathbf{v}_k^T$ ,  $\mathbf{x}_{2k} = \mathbf{v}_k - \mathbf{v}_k^T$ ,  $k = 1, \dots, K$  fi
(3)  $\mathbf{x}_k = \mathbf{P} \mathbf{x}_k \mathbf{Q}$ ,  $k = 1, \dots, 2K$ 
(4)  $M_{i-1} = 0$ ,  $M_i = 2K$ 
(5) for  $i = 0$ , until convergence or restart do
(6) orthonormalize vectors:  $\vec{x}_m \cdot \vec{x}_{m'} = \delta_{m,m'}$ ,  $m, m' = 1, \dots, M_i$ 
(7) for  $m = M_{i-1} + 1$  to  $M_i$  do
(8)  $\vec{s}_m = \mathbb{L}^{sh} \vec{x}_m$ 
(9)  $\mathbf{t}_m^q = \mathbf{P} \mathbf{s} \mathbf{Q} + (\mathbf{Q} \mathbf{s} \mathbf{P})^T$ ,  $\mathbf{t}_m^p = \mathbf{P} \mathbf{s} \mathbf{Q} - (\mathbf{Q} \mathbf{s} \mathbf{P})^T$ 
(10) end
(11) for  $m, m' = 1$  to  $M_i$  do
(12)  $\tilde{T}_{m,m'} = \vec{t}_m^p \cdot \vec{x}_{m'}$ ,  $\tilde{K}_{m,m'} = \vec{t}_m^q \cdot \vec{x}_{m'}$ 
(13) end
(14)  $\tilde{\mathbf{D}} = \tilde{\mathbf{T}}^{1/2} \tilde{\mathbf{K}} \tilde{\mathbf{T}}^{1/2}$ 
(15) solve  $\tilde{\mathbf{D}} \vec{u} = \omega \vec{u}$ ,
(16)  $\tilde{\mathbf{R}} = \tilde{\mathbf{T}}^{1/2} \mathbf{U}$ ,  $\tilde{\mathbf{L}} = \tilde{\mathbf{K}} \tilde{\mathbf{R}}$ ,  $M_{i-1} = M_i$ 
(17) for  $k = 1$  to  $K$  do
(18)  $\Omega_k = \sqrt{\omega_k}$ 
(19)  $\vec{q}_k = \sum_j^{M_i} \tilde{R}_{j,k} \vec{x}_k$ ,  $\vec{p}_k = \sum_j^{M_i} \frac{\tilde{L}_{j,k}}{\Omega_k} \vec{x}_k$ 
(20)  $\mathbf{p}_k = \mathbf{P} \mathbf{p}_k \mathbf{Q}$ ,  $\mathbf{q}_k = \mathbf{P} \mathbf{q}_k \mathbf{Q}$ 
(21)  $\vec{p}_k = \frac{\vec{p}_k}{\sqrt{|\vec{p}_k \cdot \vec{q}_k|}}$ ,  $\vec{q}_k = \frac{\vec{q}_k \text{sgn}\{|\vec{p}_k \cdot \vec{q}_k|\}}{\sqrt{|\vec{p}_k \cdot \vec{q}_k|}}$ 
(22)  $\vec{s}_k^p = \mathbb{L}^{sh} \vec{p}_k$ ,  $\vec{s}_k^q = \mathbb{L}^{sh} \vec{q}_k$ 
(23)  $\mathbf{s}_k^p = \mathbf{P} \mathbf{s}_k^p \mathbf{Q} - (\mathbf{Q} \mathbf{s}_k^p \mathbf{P})^T$ ,  $\mathbf{s}_k^q = \mathbf{P} \mathbf{s}_k^q \mathbf{Q} + (\mathbf{Q} \mathbf{s}_k^q \mathbf{P})^T$ 
(24)  $\vec{r}_k^q = \vec{s}_k^p - \Omega_k \vec{q}_k$ ,  $\vec{r}_k^p = \vec{s}_k^q - \Omega_k \vec{p}_k$ 
(25)  $\epsilon_k = \sum_{n=1}^{N^2} (\vec{r}_k^q)_n^2 + (\vec{r}_k^p)_n^2$ 
(26)  $\mathbf{v}_k = 0.5(\mathbf{q}_k + \mathbf{p}_k + (\mathbf{q}_k - \mathbf{p}_k)^T)$ 
(27) if  $\epsilon_k < \eta$ ,  $\mathbf{v}_k$  is converged vector
(28) else  $\vec{x}_{M_i+1} = \vec{r}_k^q$ ,  $\vec{x}_{M_i+2} = \vec{r}_k^p$ ,  $M_i = M_i + 2$  fi
(29) end
(30) end

```

SCHEME 3. Modified Davidson algorithm.

small irregularities, such as those associated with an incomplete sparse linear algebra. In this respect, it is worth noting the related but rather formal work of Simoncini and Elden<sup>90</sup> and Notay<sup>91</sup> on the inexact RQI.

Scheme 3 summarizes the RQI approach which employs a conventional Polak–Ribière<sup>92</sup> nonlinear conjugate gradient algorithm<sup>93</sup> and an analytic line search. Compared to the related Hermitian TDA problem, the RPA eigenstructure requests that the conventional dot product and the Ritz functional need to be replaced with the indefinite inner product [Eq. (15)] and the Thouless functional [Eq. (17)], respectively. The algorithm starts with the trial vector  $\vec{x}$  [line (2)] converging to the true eigenvector in the course of iteration. The action of the Liouville operator onto  $\vec{x}$  [line (6)] is the most CPU consuming step in the algorithm. Consequently, the value of the Thouless functional is calculated in line (8)

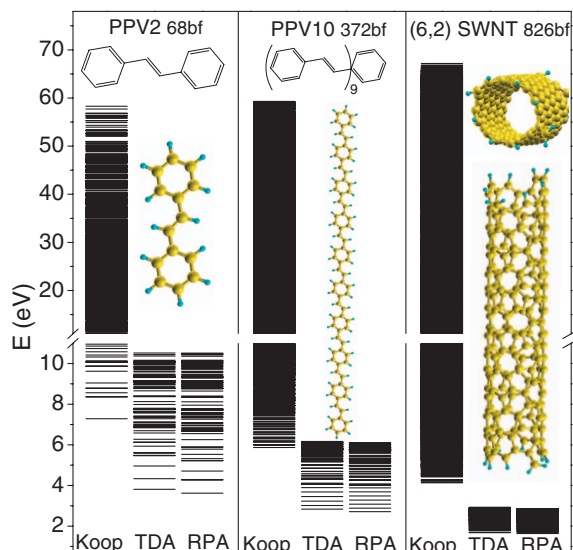


FIG. 1. (Color) Characteristic DOS in representative molecules, PPV2, PPV10, and (6,2) SWCNT, which have increasing numbers of basis functions, i.e., 68, 372, and 826 basis functions, respectively. The insets show the respective molecular structures.

and the residual norm is evaluated in line (9). Line (10) checks if the convergence criteria have been fulfilled. The algorithm further generates the gradient  $\vec{g}$  [line (11)] and projects it to the interband subspace [line (12)]. The conjugate gradient  $\vec{p}$  is calculated in lines (13) and (14), and the corresponding intermediate  $\vec{t}$  is evaluated in line (15), followed by analytic line search [line (17)] to determine the optimal step size  $\lambda$ , as described below. Finally, the approximate eigenvector  $\vec{x}$  is updated in line (18) and is projected on to the interband subspace [line (19)].

The optimal value of the line search parameter  $\lambda$  is obtained from the extremum of  $\Omega[\vec{x}=\vec{x}+\lambda\vec{p}]$ . Setting the first derivative to zero and solving for  $\lambda$  leads to the quadratic equation with solutions

$$\lambda_{\pm} = \frac{-b \pm \sqrt{b^2 - 4ac}}{2ac}, \quad (30)$$

where

$$a = \langle \vec{p}, \vec{t} \rangle (\langle \vec{p}, \vec{x} \rangle + \langle \vec{x}, \vec{p} \rangle) - \langle \vec{p}, \vec{p} \rangle (\langle \vec{p}, \vec{s} \rangle + \langle \vec{x}, \vec{t} \rangle), \quad (31)$$

$$b = 2\langle \vec{p}, \vec{t} \rangle \langle \vec{x}, \vec{x} \rangle - 2\langle \vec{x}, \vec{s} \rangle \langle \vec{p}, \vec{p} \rangle, \quad (32)$$

$$c = \langle \vec{x}, \vec{x} \rangle (\langle \vec{p}, \vec{s} \rangle + \langle \vec{x}, \vec{t} \rangle) - \langle \vec{x}, \vec{s} \rangle (\langle \vec{p}, \vec{x} \rangle + \langle \vec{x}, \vec{p} \rangle). \quad (33)$$

We note that  $\lambda_+$  is the minimizer, which is the solution used in line (18).

#### IV. NUMERICAL TESTS

For numerical tests of the four outlined algorithms we use a semiempirical TD-HF technique,<sup>23,94–96</sup> which allows us to consider realistic large molecular systems and to closely mimic numerical conditions of those encountered with large-scale first principles codes. All numerical tests are based on the collective electronic oscillator (CEO) code.<sup>23,94–96</sup> This package combines commonly used semi-

```

(1) for  $k = 1$  to  $K$  do
(2)   Generate trial vector,  $\vec{x}$ ,
(3)    $\mathbf{x} = \mathbf{P} \mathbf{x} \mathbf{Q}$ 
(4)   for  $i = 0$ , until convergence do
(5)      $\vec{x} = \frac{\vec{x}}{\sqrt{|\langle \vec{x}, \vec{x} \rangle|}}$ 
(6)      $\vec{s} = \mathbb{L}^{sh} \vec{x}$ 
(7)      $\mathbf{s} = \mathbf{P} \mathbf{s} \mathbf{Q} + \mathbf{Q} \mathbf{s} \mathbf{P}$ 
(8)      $\Omega = \frac{\langle \vec{x}, \vec{s} \rangle}{|\langle \vec{x}, \vec{x} \rangle|}$ 
(9)      $\epsilon = \sum_{n=1}^{N^2} (\Omega \vec{x}_n - \vec{s}_n)^2$ 
(10)    if  $\epsilon < \eta$ ,  $\Omega_k = \Omega$ ,  $\vec{v}_k = \vec{x}$ , exit, fi
(11)     $\vec{g}_i = 2(\vec{s} - \Omega \vec{x})$ 
(12)     $\mathbf{g}_i = \mathbf{P} \mathbf{g}_i \mathbf{Q} + \mathbf{Q} \mathbf{g}_i \mathbf{P}$ 
(13)     $\beta = \max \left\{ 0, \frac{\langle \vec{g}_i - \vec{g}_{i-1}, \vec{g}_i \rangle}{\langle \vec{g}_{i-1}, \vec{g}_{i-1} \rangle} \right\}$ 
(14)     $\vec{p}_i = \vec{g}_i + \beta \vec{p}_{i-1}$ 
(15)     $\vec{t} = \mathbb{L}^{sh} \vec{p}_i$ 
(16)     $\mathbf{t} = \mathbf{P} \mathbf{t} \mathbf{Q} + \mathbf{Q} \mathbf{t} \mathbf{P}$ 
(17)     $\lambda_i = \arg \min_{\lambda} \Omega[\vec{x} + \lambda \vec{p}_i]$ 
(18)     $\vec{x} = \vec{x} + \lambda_i \vec{p}_i$ 
(19)     $\mathbf{x} = \mathbf{P} \mathbf{x} \mathbf{Q} + \mathbf{Q} \mathbf{x} \mathbf{P}$ 
(20)  end
(21) end

```

Scheme 4. Asymmetric Rayleigh Quotient Iteration (RQI).

empirical models [such as AM1, PM3, intermediate neglect of differential overlap/spectroscopy (INDO/S) with RPA and TDA formalisms. Conventional MO-based implementation of Davidson's algorithm makes CEO computation of an excited state manifold not substantially more numerically demanding than ground state calculations. Consequently, excited state calculations of molecular systems up to thousands of atoms are routinely possible. The CEO modeling of electronic spectra has been successfully applied in the past to calculate optical properties of a variety of conjugated chromophores such as polymers (also with donors and acceptors), dendrimers, biological light-harvesting complexes, and carbon nanotubes.<sup>23,94–98</sup>

The three molecular systems shown in Fig. 1 have been used to test the excited state algorithms, namely, phenylenevinylene oligomers with two and ten repeat units (PPV2 and PPV10), and a finite segment of a (6,2) single-walled carbon nanotube (SWCNT). These are conjugated molecular systems, in which all low-energy excited states are delocalized  $\pi-\pi^*$  electronic excitations strongly susceptible to external electric field perturbations such as laser light (for detailed CEO studies of similar molecules, see, for instance, Refs. 23 and 95–97). The ground state geometries of all molecules are optimized using the semiempirical Austin model 1 (AM1) Hamiltonian,<sup>99</sup> which adequately reproduces the molecular ground state geometries, particularly in hydrocarbon compounds. In this article, for all CEO calculations of excited

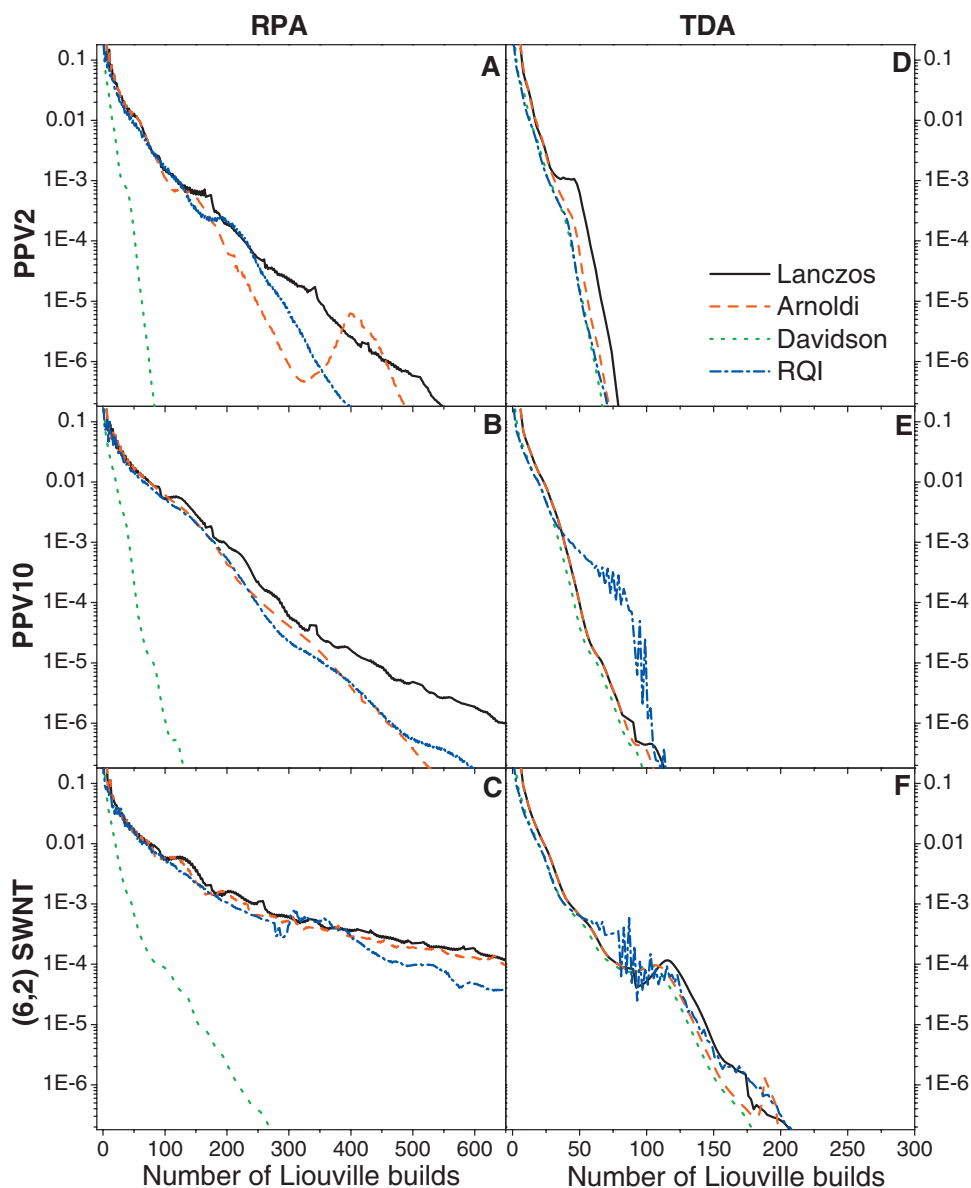


FIG. 2. (Color) Convergence rates  $\varepsilon$  of the first excited state in the absence of numerical noise in the RPA and TDA methods. The same random guess is used in all calculations. The horizontal axis (number of Liouville builds) shows the associated numerical expense. For all four algorithms, the plot shows near-exponential convergence  $\varepsilon$  as a function of numerical expense in the quasixact algebra condition (i.e., standard double precision accuracy). However, the rates of convergence are not the same for different methods.

states we use Zerner's INDO/S model<sup>100–102</sup> specifically parametrized to reproduce spectroscopic observables. We focus solely on the properties of singlet excited states built by RPA or TDA approaches from the reference singlet ground state. The outlined terminology also allows calculation of triplet excitations by accounting for proper spin indices [e.g., see, Eqs. (4)–(6)]. More complex approaches, such as spin-flip techniques, consider various spin multiplicities in the ground and excited states.<sup>103,104</sup>

The density of states (DOS) of test molecules is shown in Fig. 1. The Koopmans transition energies typically lying in the range of 2–70 eV represent all possible single-electron transitions from occupied to valence molecular orbitals. We also calculate the first 100 excited states in all molecules using a conventional MO algorithm in the CEO code for TDA and RPA methods. As expected, inclusion of electronic correlations shifts the Koopmans transition energies to the red

substantially. In contrast, the difference between TDA and RPA excitation energies is minimal. For reference, the calculated first excited state transition energy and averaged DOS among the first 100 excited states in the RPA approach are 3.62 eV and 70 meV in PPV2, 2.71 eV and 33 meV in PPV10, and 1.64 eV and 12 meV in (6,2) SWCNT. Very similar values are obtained in the TDA method. Such a decrease in the optical gap and increase of DOS with increasing molecular size augment the numerical complexity of approximate diagonalization of the Liouville superoperator.

We coded all four algorithms described in Schemes 1–4 into the CEO package by deliberately choosing the default orthogonal atomic basis set for all numerical operations, i.e., completely bypassing the MO representation. This implementation still uses dense linear algebra and a conventional  $\mathcal{O}(N^3)$  approach to HF theory. To simulate inexact algebra conditions we further impose an artificial numerical noise on

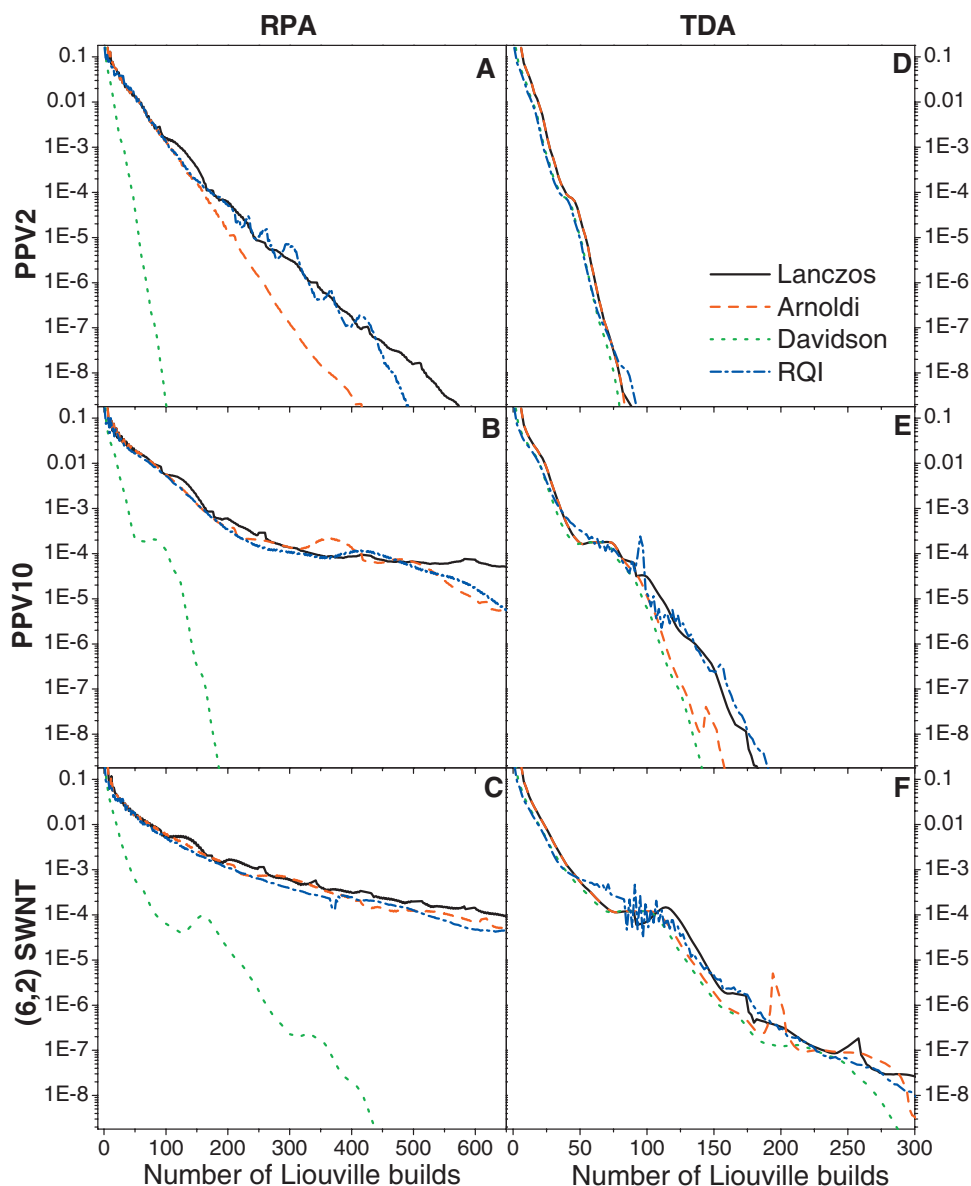


FIG. 3. (Color) Same as Fig. 2 but for the tenth excited state.

the matrix elements of Liouville builds [Eq. (27)] as

$$(\mathbb{L}^{\text{sh}}\vec{x})_n^{\text{noise}} = (\mathbb{L}^{\text{sh}}\vec{x})_n + \xi_n \max_n |(\mathbb{L}^{\text{sh}}\vec{x})_n|, \quad n = 1, \dots, N^2, \quad (34)$$

where randomly generated numbers  $\xi_n$  do not exceed the chosen noise threshold  $\tau$ . Finally, for all numerical benchmarks we limit the expansion subspace for trial vectors to 200 vectors in Lanczos, Arnoldi, and Davidson algorithms. Once the maximum expansion is reached, the calculations restart using the updated initial guesses of eigenvectors. This should simulate actual conditions by preserving memory and capping I/O. Unless specified otherwise, random guesses for trial vectors have been used in all simulations.

Convergence rates (i.e., the respective residual norms  $\varepsilon$ ) of the first excited state in three molecules are illustrated in Fig. 2. As expected, larger molecules with denser spectra require more iterations (compare panels A–C and D–F in Fig. 2). Even though Lanczos and Arnoldi iterations should

coincide in the limit of exact algebra, in practice, their convergence rates become notably different for  $n \geq 50$  iterations (i.e., about 100 Liouville builds). Compared to the RPA framework (left column in Fig. 2), the convergence is much faster in the TDA approach (right column in Fig. 2) due to Hermitian virtues. Interestingly, all algorithms exhibit a very similar convergence rate for TDA for all three molecules, where Davidson's approach shows slightly faster convergence. The situation is different in RPA. Here Davidson's approach displays much faster convergence, whereas the other three algorithms show quite similar and disproportionately slower (compared to their performance in TDA) convergence. To rationalize this trend we recall that Arnoldi, Lanczos, and RQI algorithms deal with the original non-Hermitian RPA eigenproblem given by Eq. (8) or Eq. (20), whereas the Davidson method works with the corresponding Hermitian representation written in the form of Eq. (22) or Eq. (23). Consequently, the numerical penalty when going from TDA to RPA is relatively small (factors of 1.5–2) in the

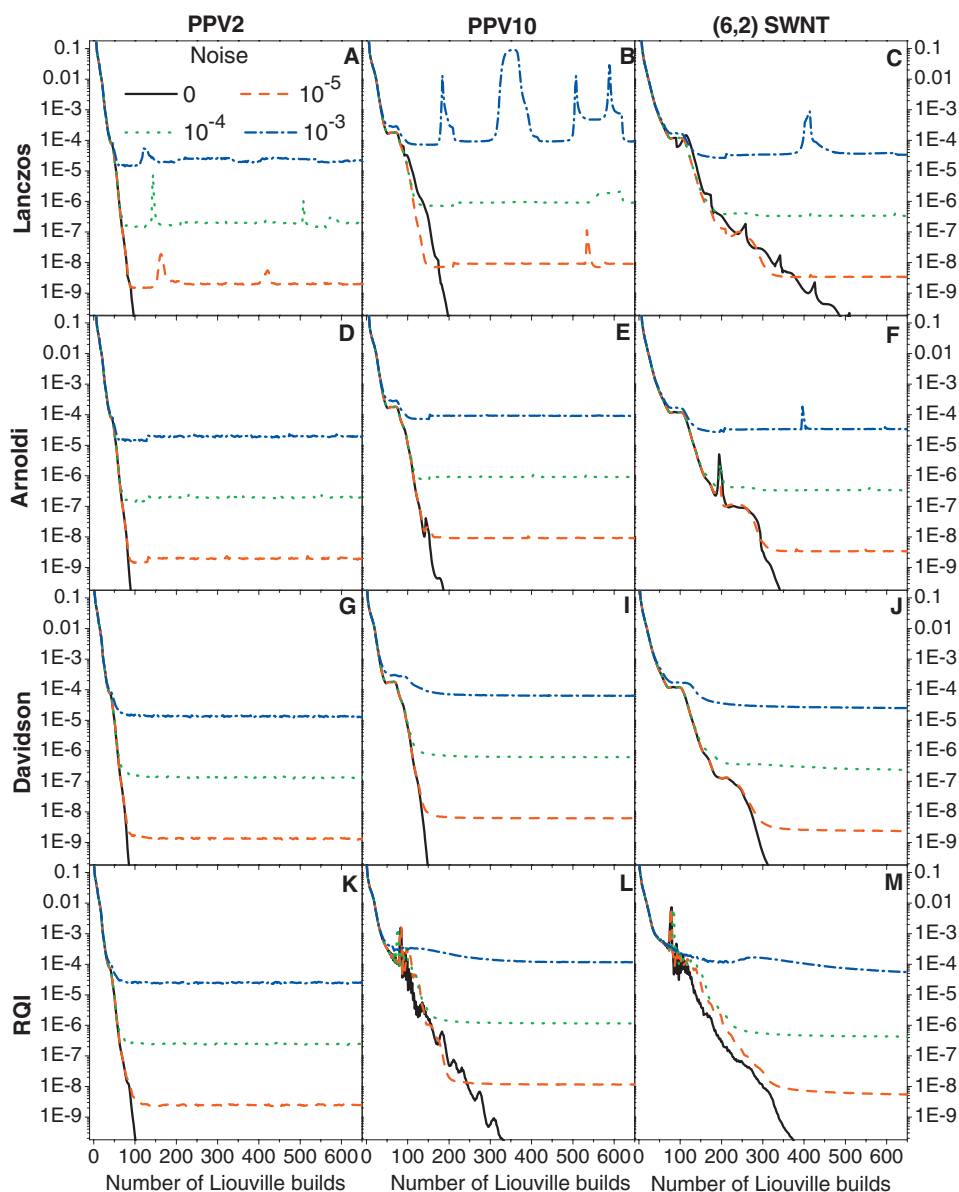


FIG. 4. (Color) Convergence rates  $\varepsilon$  of the first excited state in the presence of numerical noise in the TDA method. The same random guess is used in all calculations. The horizontal axis (number of Liouville builds) shows the associated numerical expense. We apply random noise at  $\tau=0$ ,  $10^{-5}$ ,  $10^{-4}$ , and  $10^{-3}$  levels, which approximately spans typical numerical cutoff thresholds in the linear scaling schemes. Ideally, the convergence parameter should reach a certain floor defined by the numerical noise and should stay nearly constant at this value for a number of iterations.

Davidson algorithm due to augmentation of the vector space with hp transitions. The situation is much worse for other algorithms. However, it is possible to reformulate each technique using the respective Hermitian framework outlined in Sec. II D, which potentially should improve their performance for the RPA problem.

The same trends are observed for convergence for the higher excited states in exact algebra conditions. For example, Fig. 3 shows convergence rates obtained for the tenth eigenvector. As expected, the numerical expense is moderately increased since the algorithms deal with denser eigenspectra. We also observe nonmonotonic convergence. The flat plateaus in the plots (e.g., panels B and E in Fig. 3) appear because the algorithm frequently quasiconverges to the higher-energy excited state eigenvector and can get stuck there for several iterations. In our experience, a Wilkinson shift works very well and does not introduce any numerical

problems or instabilities in both exact and inexact algebra. Indeed, the 100 excited states shown in Fig. 1 have been calculated using a Wilkinson shift in batches of ten states each in the conventional MO implementation. We previously reported calculations of up to 300 excited states in carbon nanotube segments<sup>97</sup> confirming the robustness of this approach.

We next examine the effect of imposed numerical noise, which is an inevitable complication arising in all linear scaling algorithms. Here we focus only on the lowest state. The trends for the higher excited states are found to be the same. Figures 4 and 5 show the convergence rates for TDA and RPA approaches, respectively. We notice that the Lanczos approach becomes extremely unstable and frequently breaks down with subsequent spontaneous restart (panels A–C in Figs. 4 and 5). Sometimes calculations do not converge. As was pointed out in previous studies,<sup>79,88</sup> this occurs because

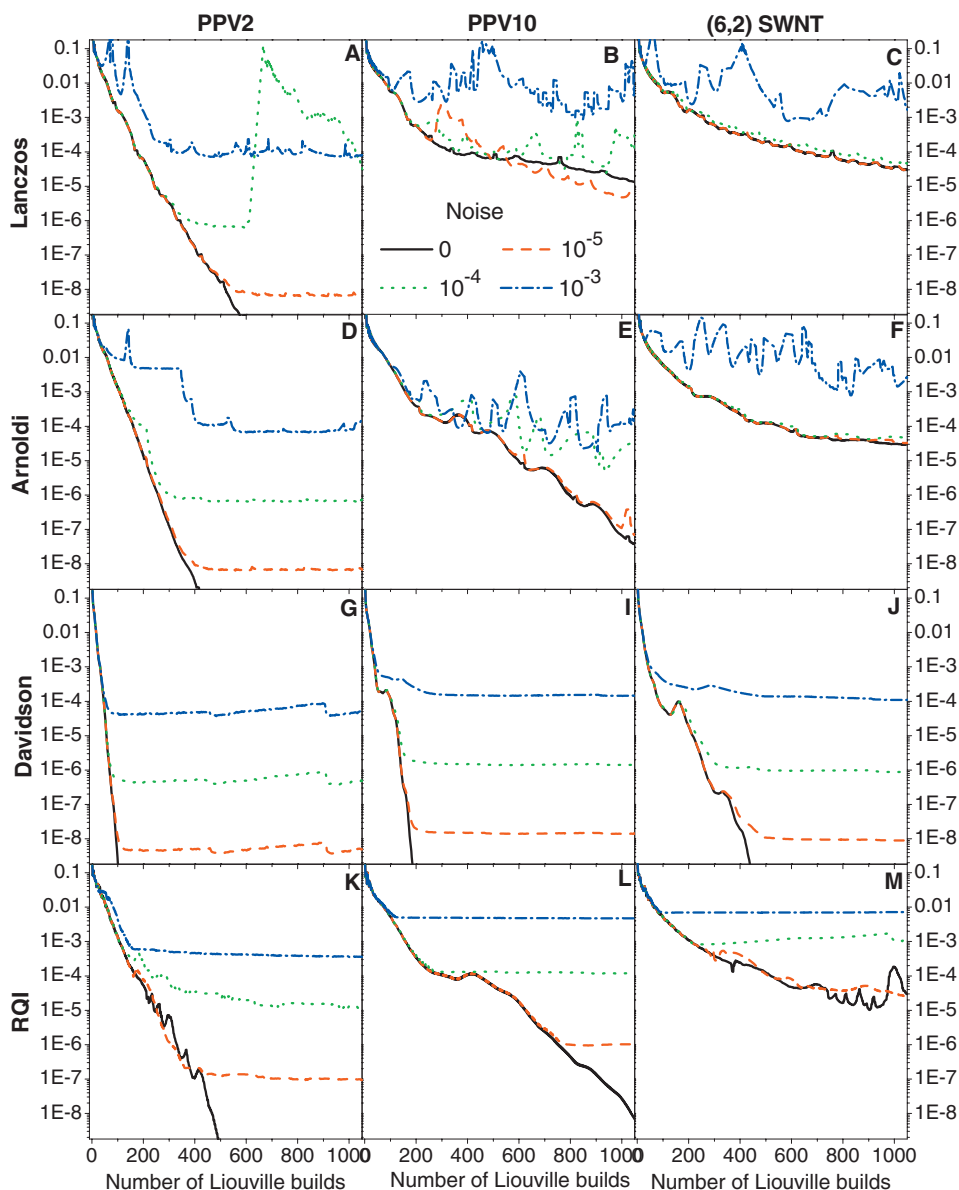


FIG. 5. (Color) Same as Fig. 4 but in the RPA method.

the numerical error accumulates due to the specific Lanczos recursion relations (28) and (29). This accumulation of the error breaks down the orthogonality in the chain of Lanczos vectors, which in turn breaks the algorithm. This problem virtually prevents practical utilization of the Lanczos algorithm in inexact algebra conditions. Even though the numerical error accumulates in Arnoldi's method as well, the explicit orthogonalization of the vectors helps stabilize the algorithm. Consequently, we observe only infrequent spontaneous restarts of the Arnoldi algorithm in the TDA framework (see panels D–F in Fig. 4). However, the same problem is again noticeable for Arnoldi in the RPA at high noise levels (see panels D–F Fig. 5). In contrast, both Davidson's and RQI algorithms display near ideal behavior with respect to the numerical noise in TDA as shown Fig. 4, panels G–M. These methods exhibit slightly less smooth behavior in the RPA (see panels G–M in Fig. 5). Here slow convergence of RQI for large molecules becomes particularly problematic (panel M in Fig. 5).

In Fig. 6 we summarize the relative amount of net numerical expense required to calculate several excited states. This plot clearly illustrates that numerical expense scales approximately linearly with the number of calculated excited states in all algorithms. It also confirms our previous observation that the Davidson algorithm that finds states one by one is significantly faster than both Arnoldi and RQI approaches in the RPA (left column in Fig. 6). This advantage becomes less pronounced the TDA (right column in Fig. 6). Moreover, the Davidson algorithm that finds all states simultaneously shows the fastest convergence for both the RPA and TDA. The higher-lying excited states are “sampled” during the eigenvector iterations, and this information remains built into the vector expansion space, which accelerates overall convergence of several states that are iterated together.

We lastly investigate the dependence of the convergence rates on the initial guess for the trial vectors. The results for different guesses obtained with Davidson's algorithm are illustrated in Fig. 7. Currently Koopmans transitions between

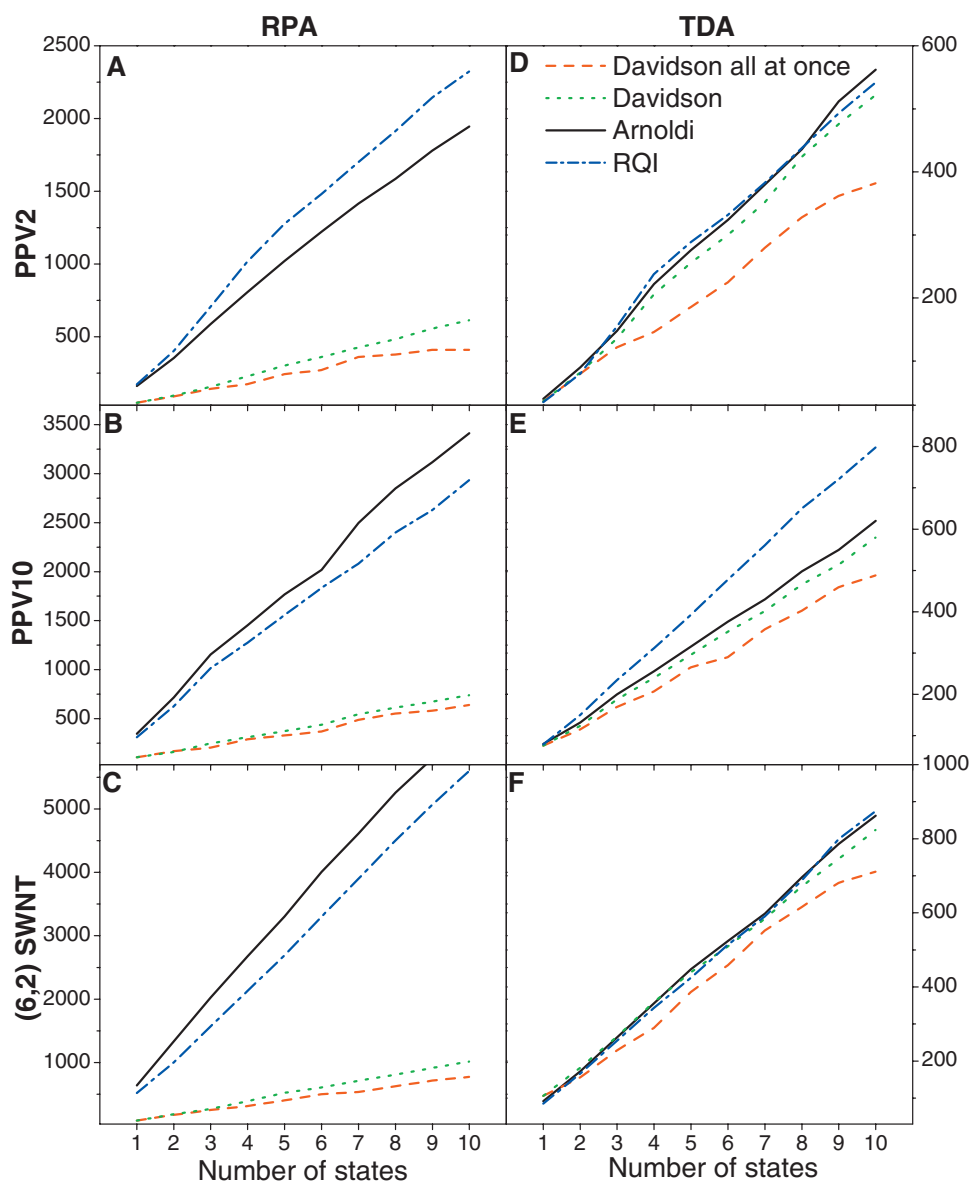


FIG. 6. (Color) Variation of numerical expense with the number of calculated states in different algorithms in exact algebra. The vertical axis shows the number of associated Liouville builds.

occupied-virtual MOs are commonly used initial approximations in a variety of codes. We first discuss this approach combined with Davidson's preconditioning available in the MO representation as a reference point. Indeed this combination guarantees the fastest convergence rates in all molecules (see Fig. 7). Such accelerated convergence rates are typical for modern MO-based codes, which linear scaling techniques need to match. Removing Davidson's preconditioning slows down the convergence rates by factors of 2–3 (see Fig. 7). As expected, the simplest random guess for the orbital-free representation ensures the slowest convergence in the pack. More intelligent (but still readily available) diagonally dominant guesses work better. Here, as an initial guess we use matrices  $x_{ij} = \xi_{ij} P_{ij}$ , where  $\xi_{ij}$  is a random number spanning  $[-1, 1]$  and  $P_{ij}$  is the respective matrix element of the ground state density matrix. This guess roughly has the same off-diagonal spatial extent as the ground state density matrix, which is readily available from the HF calculations. Indeed, compared to the completely random guess this

approximation provides universally faster convergence across the board and is closer to the Koopmans guess convergence. Finally we use density matrices  $\mathbf{P}^{(1)}$  (linear response). Such quantities up to third order in the field recently became available for calculations<sup>14–16,82</sup> in the linear scaling regime.<sup>19,83</sup> We observe that such a guess provides very fast convergence, notably, even faster than the HOMO-LUMO guess (see Fig. 7). However, we note that such guesses may not be very efficient for high-energy optically inactive electronic transitions.

## V. SUMMARY

Computation of TD-SCF electronic excitations within the linear scaling regime necessarily demands an orbital-free representation. This poses new requirements and challenges for numerical algorithms. Even though the formalism utilizing advanced projection techniques and the  $J$ -symmetric scalar product (see Sec. II) allows calculation in orbital indepen-

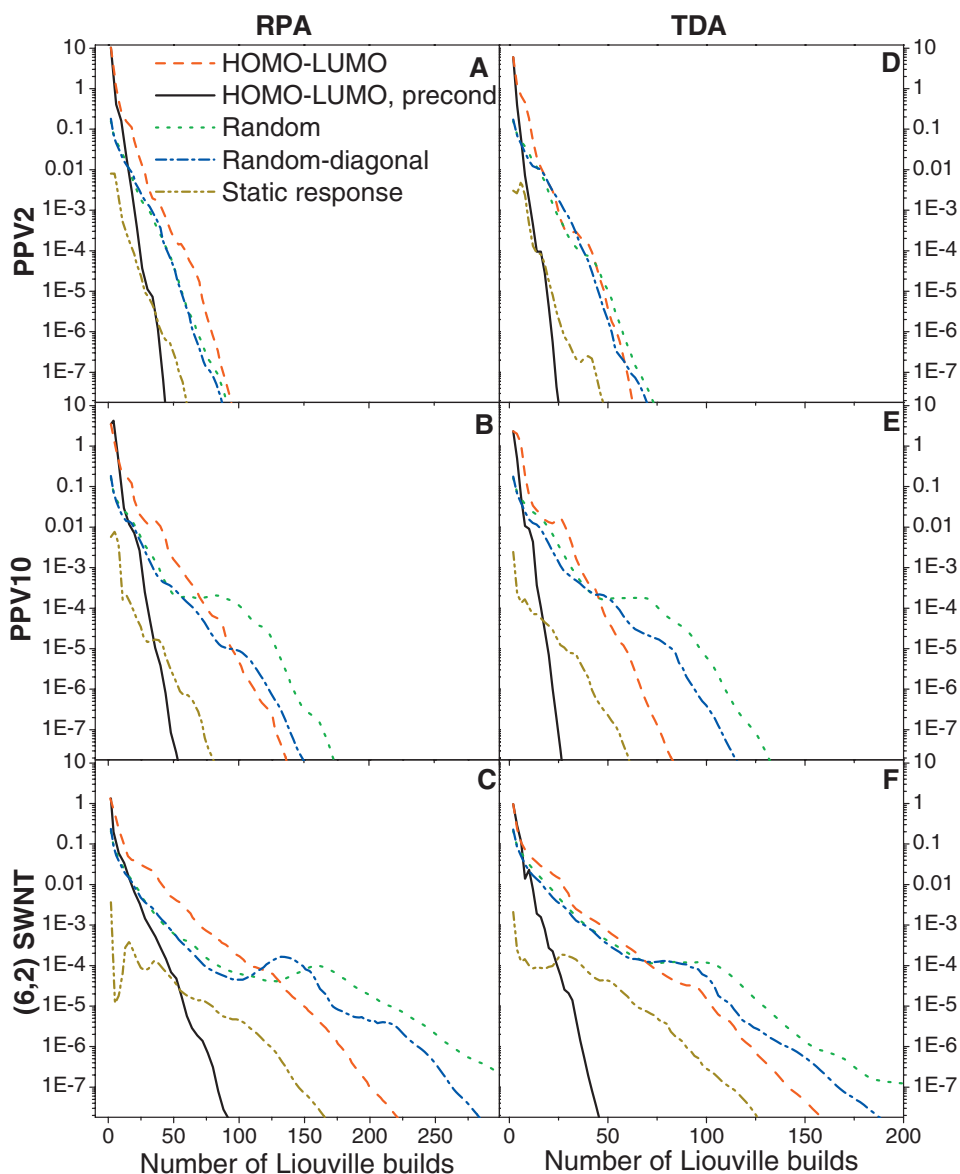


FIG. 7. (Color) Convergence rates  $\varepsilon$  of the first excited state in the absence of numerical noise as a function of the initial guess in Davidson's algorithm. Five different approximations are tested: Koopmans single-electron transitions between occupied-virtual MOs (HOMO-LUMO), Koopmans guesses with Davidson's preconditioning (HOMO-LUMO preconditioning), random guesses (random), diagonally dominant random guesses (random diagonal), and density matrices  $P^{(1)}$  induced in response to a static external electric field (linear response).

dent representations, much study needs to be done on the iterative algorithms. For example, an algorithm's performance and stability in inexact algebra conditions becomes critical to achieving linear scaling. In this study we directly compare the performance of several different approaches commonly utilized in sparse algebra and related quantum chemistry methodologies. Even though benchmarking is done using conventional dense matrix algebra, we use an orbital-free representation and simulate typical numerically noisy conditions of linear scaling techniques. Utilization of a semiempirical TD-SCF framework allows testing the iterative techniques on realistic molecules of various sizes with different spectral densities.

We found that accumulation of numerical errors due to noise in the recursive Krylov subspace procedures is a severe issue. Consequently, the Lanczos algorithm becomes unstable due to fast loss of orthogonality in the expansion vec-

tors. Similar problems exist to a lesser extent for the Arnoldi technique. RQI does not accumulate numerical error and shows reasonably fast convergence and stability for Hermitian TDA case. In contrast, RQI minimization of the Thouless functional [Eq. (17)] in the RPA case proved to be problematic with slow and unreliable convergence. Likely, reformulation of the algorithm in the coordinate-momentum variables (Sec. II D) and using Hermitian analogs of the RPA problem [Eq. (22) or Eq. (23)] could help. Even without preconditioning, Davidson's algorithm in the orbital-free representation proved to be the fastest approach; it shows excellent stability with respect to noise and does not accumulate numerical errors (in contrast to the Arnoldi and Lanczos techniques, the Davidson method does not build a nested Krylov subspace). Using the Davidson algorithm to compute several states at once (block method) reduced numerical expense even further. We also found that the quality of the

initial guess for the excitation vector (transition density matrix) is critical for improved convergence and stability. Simple random diagonally dominant guesses, which roughly imitate the spatial extent of the ground state density matrix, are efficient and work well. Electric field-induced density matrices from response theory are even better guesses. Finally, we expect that the Wilkinson shift<sup>81</sup> will be a robust approach allowing computation of higher-energy excited states if blocklike calculations are prohibitive due to memory and I/O requirements.

## ACKNOWLEDGMENTS

This work was supported by the U.S. Department of Energy and Los Alamos LDRD funds. Los Alamos National Laboratory was operated by the Los Alamos National Security, LLC, for the National Nuclear Security Administration of the U.S. Department of Energy under Contract No. DE-AC52-06NA25396. We acknowledge support of the Center for Integrated Nanotechnology (CINT) and the Center for Nonlinear Studies (CNLS). C.M.I. thanks Andri Arnaldsson for useful discussions.

- <sup>1</sup>A. Szabo and N. S. Ostlund, *Modern Quantum Chemistry: Introduction to Advanced Electronic Structure Theory* (McGraw-Hill, New York, 1989).
- <sup>2</sup>D. B. Cook, *Handbook of Computational Quantum Chemistry* (Oxford University Press, New York, 1998).
- <sup>3</sup>C. J. Cramer, *Essentials of Computational Chemistry* (Wiley, West Sussex, England, 2002).
- <sup>4</sup>C. F. Guerra, J. G. Snijders, G. Veldev, and E. J. Baerends, *Theor. Chem. Acc.* **99**, 391 (1998).
- <sup>5</sup>S. Goedecker, *Rev. Mod. Phys.* **71**, 1085 (1999).
- <sup>6</sup>E. Schwegler, M. Challacombe, and M. Head Gordon, *J. Chem. Phys.* **106**, 9708 (1997).
- <sup>7</sup>M. Challacombe, *J. Chem. Phys.* **110**, 2332 (1999).
- <sup>8</sup>M. C. Strain, G. E. Scuseria, and M. J. Frisch, *Science* **271**, 51 (1996).
- <sup>9</sup>P. Salek, S. Høst, L. Thøgersen, P. Jørgensen, P. Manninen, J. Olsen, B. Jansík, S. Reine, F. Pawłowski, and E. Tellgren, *J. Chem. Phys.* **126**, 114110 (2007).
- <sup>10</sup>G. Galli, *Curr. Opin. Solid State Mater. Sci.* **1**, 864 (1996).
- <sup>11</sup>P. Ordejón, *Comput. Mater. Sci.* **12**, 157 (1998).
- <sup>12</sup>G. Scuseria, *J. Phys. Chem.* **103**, 4782 (1999).
- <sup>13</sup>S. Y. Wu and C. S. Jayanthi, *Phys. Rep.* **358**, 1 (2002).
- <sup>14</sup>V. Weber, A. M. N. Niklasson, and M. Challacombe, *Phys. Rev. Lett.* **92**, 193002 (2004).
- <sup>15</sup>A. M. N. Niklasson and V. Weber, *J. Chem. Phys.* **127**, 064105 (2007).
- <sup>16</sup>A. M. N. Niklasson and M. Challacombe, *Phys. Rev. Lett.* **92**, 193001 (2004).
- <sup>17</sup>V. Weber, A. M. N. Niklasson, and M. Challacombe, *J. Chem. Phys.* **123**, 044106 (2005).
- <sup>18</sup>H. Xiang, J. Yang, J. Hou, and Q. Zhu, *Phys. Rev. Lett.* **97**, 266402 (2006).
- <sup>19</sup>A. M. N. Niklasson and M. Challacombe, *Phys. Rev. Lett.* **92**, 193001 (2004).
- <sup>20</sup>G. Onida, L. Reining, and A. Rubio, *Rev. Mod. Phys.* **74**, 601 (2002).
- <sup>21</sup>M. C. Zerner, *Theor. Chem. Acc.* **103**, 217 (2000).
- <sup>22</sup>J. L. Brédas, J. Cornil, D. Beljonne, D. A. dos Santos, and Z. Shuai, *Acc. Chem. Res.* **32**, 267 (1999).
- <sup>23</sup>S. Tretiak and S. Mukamel, *Chem. Rev. (Washington, D.C.)* **102**, 3171 (2002).
- <sup>24</sup>A. D. Becke, *J. Chem. Phys.* **98**, 1372 (1993).
- <sup>25</sup>E. Runge and E. K. U. Gross, *Phys. Rev. Lett.* **52**, 997 (1984).
- <sup>26</sup>M. E. Casida, in *Recent Advances in Density-Functional Methods, Vol. 3 of Part I*, edited by D. A. Chong (World Scientific, Singapore, 1995).
- <sup>27</sup>F. Furche, *J. Chem. Phys.* **114**, 5982 (2001).
- <sup>28</sup>E. K. U. Gross, J. F. Dobson, and M. Petersilka, *Top. Curr. Chem.* **181**, 81 (1996).
- <sup>29</sup>A. Dreuw and M. Head-Gordon, *Chem. Rev. (Washington, D.C.)* **105**,

- 4009 (2005).
- <sup>30</sup>M. Guillaume, V. Liégeois, B. Champagne, and F. Zutterman, *Chem. Phys. Lett.* **446**, 165 (2007).
- <sup>31</sup>K. Burke, J. Werschnik, and E. Gross, *J. Chem. Phys.* **123**, 062206 (2005).
- <sup>32</sup>F. Furche and R. Ahlrichs, *J. Chem. Phys.* **117**, 7433 (2002).
- <sup>33</sup>J. Lindhard, *K. Dan. Vidensk. Selsk. Mat. Fys. Medd.* **28**(8) (1954).
- <sup>34</sup>D. Pines and D. Bohm, *Phys. Rev.* **85**, 338 (1952).
- <sup>35</sup>D. J. Thouless, *The Quantum Mechanics Of Many-Body Systems* (Academic, New York, 1972).
- <sup>36</sup>P. Ring and P. Schuck, *The Nuclear Many-Body Problem* (Springer-Verlag, New York, 1980).
- <sup>37</sup>E. R. Davidson, *J. Comput. Phys.* **17**, 87 (1975).
- <sup>38</sup>S. Rettrup, *J. Comput. Phys.* **45**, 100 (1982).
- <sup>39</sup>J. Olsen, H. J. A. Jensen, and P. Jørgensen, *J. Comput. Phys.* **74**, 265 (1988).
- <sup>40</sup>M. E. Casida, C. Jamorski, K. C. Casida, and D. R. Salahub, *J. Chem. Phys.* **108**, 4439 (1998).
- <sup>41</sup>R. E. Stratmann, G. E. Scuseria, and M. J. Frisch, *J. Chem. Phys.* **109**, 8218 (1998).
- <sup>42</sup>D. Rocca, R. Gebauer, Y. Saad, and S. Baroni, *J. Chem. Phys.* **128**, 154105 (2008).
- <sup>43</sup>A. F. Izmaylov, E. N. Brothers, and G. E. Scuseria, *J. Chem. Phys.* **125**, 224105 (2006).
- <sup>44</sup>J. Kussmann and C. Ochsenfeld, *J. Chem. Phys.* **127**, 054103 (2007).
- <sup>45</sup>X. Andrade, S. Botti, M. A. L. Marques, and A. Rubio, *J. Chem. Phys.* **126**, 184106 (2007).
- <sup>46</sup>S. Coriani, S. Høst, B. Jansík, L. Thøgersen, J. Olsen, P. Jørgensen, S. Reine, F. Pawłowski, T. Helgaker, and P. Salek, *J. Chem. Phys.* **126**, 154108 (2007).
- <sup>47</sup>C. Y. Yam, S. Yokojima, and G. H. Chen, *Phys. Rev. B* **68**, 153105 (2003).
- <sup>48</sup>S. Yokojima and G. H. Chen, *Chem. Phys. Lett.* **292**, 379 (1998).
- <sup>49</sup>M. Payne, M. Teter, D. Allan, T. Arias, and J. Joannopoulos, *Rev. Mod. Phys.* **64**, 1045 (1992).
- <sup>50</sup>J. P. Perdew, A. Ruzsinszky, G. I. Csonka, O. A. Vydrov, G. E. Scuseria, L. A. Constantin, X. Zhou, and K. Burke, *Phys. Rev. Lett.* **100**, 136406 (2008).
- <sup>51</sup>J. Hafner, *Comput. Phys. Commun.* **177**, 6 (2007).
- <sup>52</sup>K. I. Igemshchev, S. Tretiak, and V. Y. Chernyak, *J. Chem. Phys.* **127**, 114902 (2007).
- <sup>53</sup>M. J. Lucero, A. M. N. Niklasson, S. Tretiak, and M. Challacombe, *J. Chem. Phys.* **129**, 064114 (2008).
- <sup>54</sup>S. Mukamel, *Principles of Nonlinear Optical Spectroscopy* (Oxford, New York, 1995).
- <sup>55</sup>S. Yokojima and G. H. Chen, *Chem. Phys. Lett.* **292**, 379 (1998).
- <sup>56</sup>K. Yabana and G. F. Bertsch, *Int. J. Quantum Chem.* **75**, 55 (1999).
- <sup>57</sup>A. Tsolakidis, D. Sanchez-Portal, and R. Martin, *Phys. Rev. B* **66**, 235416 (2002).
- <sup>58</sup>F. Wang, C. Y. Yam, G. H. Chen, and K. Fan, *J. Chem. Phys.* **126**, 134104 (2007).
- <sup>59</sup>M. Lein and S. Kümmel, *Phys. Rev. Lett.* **94**, 143003 (2005).
- <sup>60</sup>A. Graham, *Kronecker Products and Matrix Calculus with Applications* (Halstead, John Wiley & Sons, New York, 1981).
- <sup>61</sup>T. H. Dunning and V. McKoy, *J. Chem. Phys.* **47**, 1735 (1967).
- <sup>62</sup>J. Paldus and J. Čížek, *J. Chem. Phys.* **60**, 149 (1974).
- <sup>63</sup>J. Oddershede and P. Jørgensen, *J. Chem. Phys.* **66**, 1541 (1977).
- <sup>64</sup>J. Linderberg and E. W. Thulstrup, *J. Chem. Phys.* **49**, 710 (1968).
- <sup>65</sup>S. Hirata, M. Head-Gordon, and R. J. Bartlett, *J. Chem. Phys.* **111**, 10774 (1999).
- <sup>66</sup>T. H. Dunning, Jr. and V. McKoy, *J. Chem. Phys.* **48**, 5263 (1968).
- <sup>67</sup>R. McWeeny and B. T. Sutcliffe, *Methods of Molecular Quantum Mechanics* (Academic, New York, 1976).
- <sup>68</sup>E. R. Davidson, *Reduced Density Matrices in Quantum Chemistry* (Academic, New York, 1976).
- <sup>69</sup>P.-O. Löwdin, *Adv. Phys.* **5**, 1 (1956).
- <sup>70</sup>P.-O. Löwdin, *Rev. Mod. Phys.* **34**, 80 (1962).
- <sup>71</sup>R. S. Mulliken, *J. Chem. Phys.* **23**, 1833 (1955).
- <sup>72</sup>A. H. R. Palser and D. E. Manolopoulos, *Phys. Rev. B* **58**, 12704 (1998).
- <sup>73</sup>A. M. N. Niklasson, *Phys. Rev. B* **66**, 155115 (2002).
- <sup>74</sup>D. J. Thouless, *Nucl. Phys.* **22**, 78 (1961).
- <sup>75</sup>V. Chernyak and S. Mukamel, *J. Chem. Phys.* **104**, 444 (1996).
- <sup>76</sup>E. V. Tsiper, *J. Phys. B* **34**, L401 (2001).
- <sup>77</sup>E. V. Tsiper, *JETP Lett.* **70**, 751 (1999).

- <sup>78</sup> Y. Saad, *Numerical Methods for Large Eigenvalue Problems* (University Press, Manchester, 1992).
- <sup>79</sup> Y. Saad, *Iterative Methods for Sparse Linear Systems* (Society for Industrial and Applied Mathematics, Philadelphia, PA, 2003).
- <sup>80</sup> B. N. Parlett, *Symmetric Eigenvalue Problem* (Prentice-Hall, Englewood Cliffs, 1980).
- <sup>81</sup> J. H. Wilkinson, *The Algebraic Eigenvalue Problem* (Clarendon, Oxford, 1965).
- <sup>82</sup> H. Larsen, P. Jørgensen, J. Olsen, and T. Helgaker, *J. Chem. Phys.* **113**, 8908 (2000).
- <sup>83</sup> A. M. N. Niklasson and V. Weber, *J. Chem. Phys.* **127**, 064105 (2007).
- <sup>84</sup> J. Cullum and R. A. Willoughby, *J. Comput. Phys.* **44**, 329 (1981).
- <sup>85</sup> G. Mei, MS thesis, Nanjing Aeronautical Institution, 1986.
- <sup>86</sup> P. Benner and H. Fassbender, *Linear Algebra Appl.* **263**, 75 (1997).
- <sup>87</sup> V. Chernyak, M. F. Schulz, S. Mukamel, S. Tretiak, and E. V. Tsiper, *J. Chem. Phys.* **113**, 36 (2000).
- <sup>88</sup> G. Golub, Proceedings of the International Congress of Mathematician, 1995 (unpublished), p. 1440.
- <sup>89</sup> A. Edelman and S. T. Smith, *BIT* **36**, 494 (1996).
- <sup>90</sup> V. Simoncini and L. Elden, *BIT* **42**, 159 (2002).
- <sup>91</sup> Y. Notay, *SIAM J. Matrix Anal. Appl.* **24**, 627 (2002).
- <sup>92</sup> E. Polak and G. Ribière, *Rev. Fr. Inform. Rech. Oper.* **3**, 35 (1969).
- <sup>93</sup> B. T. Polyak, *Zh. Vychisl. Mat. Mat. Fiz.* **9**, 807 (1969).
- <sup>94</sup> S. Mukamel, S. Tretiak, T. Wagersreiter, and V. Chernyak, *Science* **277**, 781 (1997).
- <sup>95</sup> S. Tretiak, A. Saxena, R. L. Martin, and A. R. Bishop, *Phys. Rev. Lett.* **89**, 097402 (2002).
- <sup>96</sup> S. Tretiak, V. Chernyak, and S. Mukamel, *J. Phys. Chem. B* **102**, 3310 (1998).
- <sup>97</sup> S. Kilina and S. Tretiak, *Adv. Funct. Mater.* **17**, 3405 (2007).
- <sup>98</sup> S. Kilina, S. Tretiak, S. K. Doorn, Z. Luo, F. Papadimitrakopoulos, A. Piryatinski, A. Saxena, and A. R. Bishop, *Proc. Natl. Acad. Sci. U.S.A.* **105**, 6797 (2008).
- <sup>99</sup> M. J. S. Dewar, E. G. Zoebisch, E. F. Healy, and J. J. P. Stewart, *J. Am. Chem. Soc.* **107**, 3902 (1985).
- <sup>100</sup> J. Ridley and M. C. Zerner, *Theor. Chim. Acta* **32**, 111 (1973).
- <sup>101</sup> J. D. D. Neto and M. C. Zerner, *Int. J. Quantum Chem.* **81**, 187 (2001).
- <sup>102</sup> J. D. Baker and M. C. Zerner, *Chem. Phys. Lett.* **175**, 192 (1990).
- <sup>103</sup> A. I. Krylov, *Acc. Chem. Res.* **39**, 83 (2006).
- <sup>104</sup> A. A. Golubeva, A. V. Nemukhin, S. J. Klippenstein, L. B. Harding, and A. I. Krylov, *J. Phys. Chem. A* **111**, 13264 (2007).